NATIONAL ADVISORY COMMITTEE FOR AERONAUTICS

TECHNICAL NOTE 3659

EFFECT OF LEADING-EDGE GEOMETRY ON BOUNDARY-LAYER TRANSITION AT MACH 3.1

By Paul F. Brinich

Lewis Flight Propulsion Laboratory
Cleveland, Ohio

Washington
March 1956

NATIONAL ADVISORY COMMITTEE FOR AERONAUTICS

TECHNICAL NOTE 3659

EFFECT OF LEADING-EDGE GEOMETRY ON BOUNDARY-LAYER TRANSITION AT MACH 3.1

By Paul F. Brinich

SUMMARY

The effect of leading-edge geometry on transition position, recovery-factor distribution, boundary-layer profile, and the roughness required to induce transition has been investigated at Mach 3.1 for a hollow cylinder alined with the air stream. The effect of surface-heat conductivity on the recovery-temperature distribution was also studied.

A large downstream displacement of the transition point and an increase in recovery factor were noted when a sharp leading edge was very slightly blunted. These effects were attributed to the formation of an inviscid shear layer near the surface caused by the curvature of the leading-edge shock. The boundary layer thus develops in a region of lower Mach number existing within this shock-produced shear layer. The delay in transition is predominantly an effect of a Reynolds number reduction within the reduced velocity region of the inviscid shear layer. A still larger downstream displacement of the transition point was observed for an externally beveled leading edge. This effect is only partly explained by the Reynolds number reduction within the inviscid shear layer caused by the leading-edge oblique shock.

A study of the effect of single roughness elements on transition showed that slight increases in leading-edge bluntness increased the roughness required to induce transition when transition was relatively far from the element. When transition was nearer the element, the behavior was reversed.

Studies of surface-temperature distributions on models having various surface-heat conductivities indicated that surface-heat-conduction effects could only partially account for the premature temperature rise ahead of the transition point.

INTRODUCTION

Research on transition from laminar to turbulent flows at low speeds has been distinguished by considerable difficulty in achieving a working relation between experiment and theory. At high speeds these difficulties have been accentuated by increased complexity of the flow and by instrumentation obstacles. Many of the problems presently encountered at high speeds, however, result from an incomplete knowledge of new parameters which may be important for an understanding of actual boundary-layer flows. One such parameter is the leading-edge thickness on an aerodynamic body, whether it be a flat plate, a wing, or a fuselage nose.

The effect of leading-edge thickness on the transition point is noted in references 1 and 2, where it is shown that slight increases in the bluntness of the sharp leading edge of a hollow cylinder alined with the air stream at Mach 3.1 delayed the appearance of transition. Studies of leading-edge bluntness (ref. 3) which have been made on flat-wing surfaces at Mach 4.0 also confirm the beneficial effect of bluntness on transition location. A detailed study of this effect on a cylinder at Mach 3.1 was the primary objective of this report. Various other leading-edge modifications were also studied in order to obtain an understanding of the mechanism of transition delay.

The leading-edge thickness is not the only geometric variation which controls transition location. The effect of an external bevel at the leading edge of a cylinder has been found to displace the transition point downstream (refs. 4 and 5). A similar effect has been found for cone cylindrical bodies (ref. 6) and this result has been widely reported. In view of these observations, a determination of what effect the internal angle of the leading edge has on the location of the transition point would be of interest.

In contrast to the large effect of the leading edge on transition, its effect on the laminar-boundary-layer development may seem small and unimportant. Several investigations of the effect of leading-edge thickness on the laminar-boundary-layer development have been made (refs. 1 and 7). An increase in the boundary-layer thickness for increasing leading-edge thicknesses is shown in these references, and in reference 1 a simultaneous effect on the transition point is noted. The effect of several leading-edge configurations on the laminar-boundary-layer profile near the leading edge was investigated herein.

The effect of single-roughness elements on the position of transition was investigated in reference 8 for a cylindrical model having a leading-edge thickness of 0.006 inch. Present knowledge shows that a leading edge with a thickness of such proportions has a considerable effect on the location of the transition point. This naturally raises a question about the quantitative results of reference 8 and necessitates

a recheck of the roughness results with the use of a more ideally sharp leading edge. A brief check of the effect of roughness using one of the elements tested in reference 8 with a sharper leading edge was made, and the results of this test comprise the second part of this report.

The third part of this report includes the interpretation of surface-temperature distributions in the neighborhood of transition. It is concluded in reference 2 that a substantial part of the surface-temperature rise ahead of the transition point could be accounted for by heat conduction along the surface of the cylinder. As a further check on this hypothesis, additional tests have been made using models with effective conductivities approximately 30 times less and 30 times greater than those used in reference 2. From these latter tests the validity of the conclusion reached in reference 2 could possibly be ascertained.

In addition to these three subjects, the effect of stagnation-temperature variations on transition and temperature distribution will be reported. The experimental results reported herein were obtained on hollow cylindrical models alined with the air stream. All tests were conducted in the NACA Lewis 1- by 1-foot variable Reynolds number tunnel at Mach 3.1 and for a Reynolds number range of 1×10^5 to 7×10^5 per inch.

SYMBOLS

The following symbols are used in this report:

C_p	pressure coefficient, $(p - p_\infty)/q_\infty$
h	convective heat-transfer rate, $q/(T_w - T_{ad})$
K	conduction parameter, $\frac{hx_f^2}{k_s t}\sqrt{\frac{x}{x_f}}$
k	height of roughness element, in.
k_s	conductivity of model surface
p	static pressure
q	rate of heat flow per unit area
q_∞	free-stream dynamic pressure, $\frac{1}{2}(\rho_\infty u_\infty^2)$
R	gas constant

Re_t free-stream transition Reynolds number, $\frac{u_\infty x_t}{\nu_\infty}$

$Re_{t,0}$ free-stream transition Reynolds number without roughness, $\frac{u_\infty x_{t,0}}{\nu_\infty}$

T temperature, $^\circ R$

t thickness of model shell, in.

u velocity

u/ν unit Reynolds number

x distance from leading edge, in.

y normal distance above surface, in.

α dimensionless velocity, $u/\sqrt{RT_0}$

δ boundary-layer thickness, in.

δ_k^* displacement thickness at roughness element, in.

η free-stream recovery factor, $\frac{T_w - T_\infty}{T_0 - T_\infty}$

θ dimensionless temperature ratio, $\frac{T_w - T_{ad}}{T_f - T_{ad}}$

ν kinematic viscosity

ξ dimensionless distance, x/x_f

ρ density

Subscripts:

ad adiabatic laminar value

f downstream extremity of laminar boundary layer

k conditions at roughness element

t conditions at transition point

w wall

0	stagnation conditions
1	conditions in the low Reynolds number layer
∞	free-stream conditions

APPARATUS AND PROCEDURE

Models and Instrumentation

The cylindrical model, with which the majority of the data in this report were obtained, is the same model as described in reference 2, with the exception of certain variations in the leading-edge geometry. Construction details are given in figure 1. The outer-shell material is 18-8 stainless steel. In addition to the leading edge shown, several other leading-edge shapes were also used.

Sections of the various leading edges are shown in figure 2. The same 5° leading edge included in figure 1 is shown in figure 2(a), but it is blunted. The leading edge was blunted by cutting it back perpendicular to the outside surface, resulting in leading-edge thicknesses of 0.0008, 0.0028, 0.005, 0.008, 0.016, and 0.043 inch. Figure 2(b) shows a leading edge having a 30° internal bevel, and figure 2(c), one having a 30° external bevel. The latter two edges each had thicknesses of about 0.001 inch.

The copper-shelled model which was used to find the effect of large surface conductivities was very similar to the stainless-steel model of figure 1, except that a copper shell with a 0.030-inch thickness replaced the stainless-steel shell. The Fiberglas plastic model, however, differed in construction from the others in that a Fiberglas plastic shell with a 0.09-inch thickness having the same outside diameter as the metal shells was used for the exterior surface. This outer insulating shell was separated from the inner steel supporting shell by a 0.06-inch air gap maintained by 30 rods, each with a 0.06-inch diameter, lying lengthwise on the inner shell and equally spaced about the circumference. A section showing construction details is presented in figure 3. Some mechanical modification to the leading-edge design was required, but the external shape of the model was left unchanged.

Thermocouple and static-pressure instrumentation on the external surface of the model is shown for the stainless-steel model in figure 1. Stainless-steel - constantan thermocouples were formed by soft-soldering constantan wire into small holes in the surface. The copper model had no static-pressure instrumentation, but it had thermocouple instrumentation at the same or larger intervals as the stainless-steel model.

Thermocouples for this model were formed of copper-constantan wire junctions soft-soldered into small holes in the surface. Like the copper model, the Fiberglas shell had only thermocouple instrumentation, but spaced at smaller intervals of 1/4 to 1 inch in order to sense more abrupt temperature changes. Iron-constantan thermocouples were imbedded in a 0.06-inch-diameter ball of silver solder, cemented into the surface, and finished off flush.

The surface finishes of the stainless-steel and copper models were of uniform quality and typical of smoothly polished sheet metal. The Fiberglas plastic model, on the other hand, had numerous surface defects due to the inhomogeneous structure of the Fiberglas material. Surface finishes on the three models were measured with a surface indicator equipped with a 0.0004-inch-radius stylus. This instrument gave the following average peak-to-valley distances of the surface in question:

Outer-shell material	Surface finish, μ in.
Stainless steel	10
Copper	18
Fiberglas plastic	75

In connection with variations in leading-edge geometry, another method of producing a curved-type shock (characteristic of a blunted leading edge) was desired. The method used to produce such a shock was to vary the amount of spillage at the leading edge by manipulating a conical plug at the exit of the cylinder (fig. 1).

For the brief roughness study included in this report, a single brass wire with a 0.052-inch diameter girded the model at 1.25, 2.5, or 5 inches from the leading edge.

Surface temperatures were obtained by reading the electrical outputs of the model thermocouples on a self-balancing potentiometer having a full-scale deflection of 1 millivolt. Most of the potentiometer readings were made manually; however, a digital converter with automatic cycling and punch-tape recording equipment was used toward the end of the test program to obtain the temperature distribution with greater ease.

Boundary-layer profiles were obtained from total-pressure measurements made with a boundary-layer-type pitot tube having a tip flattened to 0.007x0.06 inch. The positioning accuracy of the pitot tube is estimated to be ±0.0005 inch on the basis of repeatability of certain known measurements.

The relative accuracy between individual temperature measurements for any one temperature distribution is estimated to be within $\pm 1/4^{\circ}$ F. The maximum inconsistency in temperature measurements to be presented occurred on the copper model where reference temperatures were approximately $2\frac{1}{2}^{\circ}$ F below those obtained on the stainless-steel and Fiberglas plastic model. These inaccuracies, it should be noted, affect only the computed recovery factors and introduce no error in the determination of the transition point.

Model and tunnel-wall static pressures were measured on butyl phthalate differential manometers to an accuracy of ±0.002 pound per square inch. Stagnation pressures in the settling chamber were obtained to an accuracy of at least ±0.05 pound per square inch. Boundary-layer pitot readings obtained with mercury manometers were generally accurate to ±0.02 pound per square inch. The trend of measurements near the wall, particularly at low tunnel pressures, however, indicates that the latter figure may be too optimistic in a few instances.

Wind Tunnel and Test Conditions

The model was tested in the NACA Lewis 1- by 1-foot, variable Reynolds number, supersonic wind tunnel at Mach 3.1; this is the same test facility used in references 2 and 8. The turbulent intensity for the present tests should not, therefore, vary appreciably from the value given in references 2 and 8.

Most of the tests were conducted at unit Reynolds numbers u_{∞}/ν_{∞} of about 6.7, 3.5, 1.9, and 1.0×10^{5} per inch. Stagnation temperatures were maintained at 48° to 64° F except for one high-temperature run at 176° F. In order to obtain these unit Reynolds numbers, stagnation pressures were varied between 50 and 7 pounds per square inch absolute. Surface temperatures and static pressures were measured along the bottom of the model only.

The methods to be used in this investigation for defining the transition point involve the measurement of surface temperature and schlieren photography with short-duration exposures. Both of these methods are in current use for the study of high-speed boundary layers because they are convenient and do not affect the flow that is being investigated.

A difficulty arises in the use of the surface-temperature method for defining transition, however. The assumption used in the present report and in references 2 and 8 is that the transition point, or what may be called a point of special significance in the transition process, occurs at or near the peak surface temperature existing between the laminar- and turbulent-flow regions. Another and perhaps a more widely

accepted view is to define the beginning of the transition region rather rather than some point within that region (cf., refs. 6, 9, and 10). This is done by noting at what point the surface temperature first rises above the laminar recovery value (provided, of course, that the model is insulated). That such a procedure is not always possible is demonstrated in reference 8, where a continuously variable temperature which never did reach the low value characteristic of the laminar boundary layer was observed. The primary justification for using the peak temperature method, however, is that the transition point so defined, at least for the case of the cylinder tests made to date, actually corresponds to the mean transition point shown by the schlieren photographs.

RESULTS AND DISCUSSION

Leading-Edge Effect

Leading-edge thickness. - The effect of leading-edge thickness on the recovery-factor distribution is shown in figure 4 for a 5° internal-beveled leading edge. The outer shell on which the temperatures were measured was made of thin stainless steel. Unless stated to the contrary, all temperature measurements in this report were taken with the stainless-steel shell rather than the copper or Fiberglas-plastic shells. Recovery-factor distributions are presented for five leading-edge thicknesses, 0.0008, 0.0028, 0.005, 0.008, and 0.043 inch, and for four values of free-stream Reynolds number. Pressure distributions are also shown for three of the leading-edge thicknesses.

Two effects of leading-edge thickness are noteworthy in figure 4. The first is that the transition points (temperature maximums between the laminar and turbulent regions, indicated by crosses) are displaced downstream with increases in leading-edge thickness from 0.0008 to 0.008 inch. Further increases in leading-edge thickness to 0.043 inch produced only a very minor change in transition position. Other data obtained with a 0.016-inch leading edge, but not included in figure 4 because of an error in measuring the cold-junction temperature, showed transition at the same positions noted for the 0.008- and 0.043-inch leading edges.

The second effect is the gradual rise of the recovery factor in the laminar region with increases in leading-edge thickness. This rise is not limited (as the transition-point movement was) to values of leading-edge thickness less than 0.008 inch, but continues with increases in leading-edge thickness. In fact, for the 0.043-inch leading edge an appreciable increase in the turbulent recovery factor also appears.

Some discrepancies in the recovery-factor increase with leading-edge thickness are apparent in figure 4. For example, the 0.005-inch

edge sometimes shows an initial recovery factor higher than the 0.008-inch edge. This largely results from obtaining the data for the 0.005- and 0.0028-inch leading edge on a rebuilt model at a later date, using modified instrumentation and techniques. Recovery-factor discrepancies of 0.005 appear to be involved, which means temperature errors of about 1.5° F. These discrepancies in no way affect the location of the temperature peaks used in determining the transition position.

The pressure distributions of figure 4 indicate a fairly constant pressure along the cylinder. A slight perturbation of the pressure coefficient is apparent at about an x of 18 inches, caused by the reflected leading-edge shock from the 0.008- and 0.043-inch leading edges. This perturbation is also evident in the turbulent recovery factors, particularly for the 0.043-inch leading edge.

Internally beveled leading edge. - In order to determine whether the internal bevel angle of the leading edge had a significant effect on transition (e.g., by causing flow around the leading edge or changing the heat transfer there), a rather extreme bevel angle of 30° (less than the detachment angle) with a leading-edge thickness of 0.001 inch (shown in fig. 2(b)) was tested. The resulting recovery factor and pressure distributions at a free-stream Reynolds number of about 3.5×10^{5} per inch are shown in figure 5. Also shown for comparison are the distributions obtained for a leading edge with a 5° internal bevel and a 0.001-inch thickness.

A comparison of the results shows that the transition point is displaced downstream about 0.3 inch as the internal bevel angle is increased from 5° to 30°. Downstream displacements of almost equal magnitude occurred throughout the range of unit Reynolds number. Apparently the increased heat transfer through the 30°-beveled leading edge does not have a destabilizing effect on the laminar boundary layer. The internal bevel angle may be concluded not to be an important parameter insofar as transition is concerned.

The increase in the recovery-factor level for the 30°-beveled leading edge (fig. 5) is greatest in the initial laminar region, where the recovery factor changes from approximately 0.863 to 0.875. A much smaller increase in the turbulent region is detectable also. This increase is probably the result of greater heat transfer from the internal to the external surface of the leading-edge wedge in the case of the greater leading-edge angle.

A comparison of the pressure distributions obtained with the two leading-edge geometries shows minor differences up to about 18 inches from the leading edge. Thereafter, a large increase in pressure for the 30°-beveled leading edge takes place. The pressure rise, it is true, begins at the point where the leading-edge Mach wave reflects on the

model; but schlieren photographs do not indicate any corresponding disturbances, nor does past experience in testing this model give any hint as to the source of this large increase in pressure. This pressure rise occurred throughout the Reynolds number range and has not been accounted for.

Externally beveled leading edge. - The recovery-factor and pressure distributions for the 30°-external-beveled leading edge at a value of 3.5×10^5 per inch for u_∞/ν_∞ are also included in figure 5. This leading edge gave the greatest downstream displacement of the transition point thus far noted. Beneficial effects of an external-beveled leading edge have been observed previously in references 4 and 5 at Mach 2.15 to 3.25. Whether these effects are as great as observed in the present experiments cannot be determined from those references, since no dimensions are given for the leading-edge thickness of the internal-beveled model used as a comparison.

The presence of three peaks in the recovery-factor distribution for the external bevel may raise some doubt as to the actual location of the transition point. Numerous schlieren photographs taken simultaneously with the temperature distributions show the transition point to lie between 11 and 13 inches. The first peak at an x of 5.7 inches also appears in figures 4(b) and (c) for the 0.043-inch leading edge. No reason for its appearance is known. The third peak at a distance of 22 inches begins its rise at the point where the leading-edge shock is reflected back on the model (x = 14 in.).

The distribution of pressure coefficients for the external-beveled model (fig. 5) shows relatively constant pressure to about 14 inches from the leading edge. At the point of impingement of the strong leading-edge shock-system reflection, the pressure rises rapidly to a level near that observed with the 30°-internal-beveled leading edge.

Independent method for delaying transition. - In order to determine whether the physical presence of leading-edge thickness was necessary to delay transition, or whether it was merely necessary to reproduce the blunt leading-edge shock condition, the following experiment was performed. A detached normal-shock wave was positioned at the inlet of the cylinder having a 0.001-inch leading edge and 5°-internal-beveled angle. This was done by manipulating the conical tail plug at the end of the model. Shock positions approximating those obtained with the various leading-edge thicknesses were used.

The results showed that transition was again delayed as with the blunt leading edge. This delay was observed only at the lowest value of u_∞/ν_∞ because of certain mechanical difficulties and large heat-transfer effects from the internal subsonic flow at the higher Reynolds

numbers. The extent of the transition delay as observed from temperature distributions and schlieren photographs was very nearly equal to the delay obtained with the 0.008-inch or thicker leading edge.

Boundary-layer profiles. - Boundary-layer velocity profiles were measured at the position of the first static orifice on the model for the 0.0008-, 0.008-, and 0.043-inch leading edges and the 30° internal- and external-beveled leading edges. Plots of the various profiles are shown in figure 6 in terms of the normal distance y and a dimensionless velocity α where

$$\alpha = \frac{u}{\sqrt{RT_0}}$$

Also included in figure 6 are theoretical laminar velocity profiles computed according to reference 11, assuming an isothermal surface with no heat transfer for a free-stream Mach number of 3.1 and a distance of 2.45 inches from the leading edge. This curve is labeled I in figure 6. Curves II and III will be discussed in the following section.

A comparison of the experimental points and the theoretical curves for the sharpest leading edge with internal bevel (curve I) shows that the best agreement is attained with the 0.0008-inch leading edge having a 5° internal bevel except for a region near the wall where there appear to be errors in total-pressure measurements. The agreement for this leading edge is seen to improve as the unit Reynolds number is reduced, possibly because of the increasing ratio of the boundary-layer thickness to the probe size. A few discrepancies in the measured profiles occurring close to the wall are very likely the result of probe-wall interference or low Reynolds number effects.

The next best agreement between experiment and theory occurs for the 0.001-inch leading edge with a 30° internal bevel. The increased departure from the computed curve for the larger leading-edge angle suggests the possibility of a heat-transfer effect caused by the rising recovery temperature at the inside of the leading edge. The over-all boundary-layer thickness, however, is very close to the computed value and to that measured for the smaller leading-edge bevel.

Increasing the thickness of the leading edge to 0.008 and 0.043 inch produced larger deviations from the theoretical curves, particularly with regard to the velocity at a distance from the wall corresponding approximately to the edge of the theoretical boundary layer. This velocity decrease is large in going from the 0.0008- to the 0.008-inch leading edge and rather small in going from 0.008 to 0.043 inch. This observation ties in with a result found earlier that increases in leading-edge thickness beyond 0.008 inch had little effect in producing

further delays in transition. The free-stream Mach number of 3.1 was attained at a y of 0.12 inch for the 0.008-inch leading edge and at a y of 0.6 inch for the 0.043-inch leading edges.

The 30°-external-beveled-leading-edge results fall closer to curve I than do either of the blunted leading edges. The velocity at the predicted outer edge of the boundary layer, however, falls rather close to that for the 0.008-inch leading edge.

Explanation of transition delay and other effects. - In proposing an explanation for the effects of changes in leading-edge geometry, the following observations are considered of special significance:

(1) The downstream displacement of transition for increases in leading-edge thickness and for external bevel

(2) The downstream displacement of transition caused by a curved shock positioned ahead of a sharp leading edge

(3) Increases in laminar and occasionally turbulent recovery factor with increases in leading-edge thickness

(4) Decreasing velocity at the edge of laminar boundary layer with increasing leading-edge thickness and with external-beveled leading edge.

The existence of a leading-edge shock-produced shear layer adjacent to the model surface has been proposed to explain the preceding observations (ref. 12). Mach number profiles in this shock-produced shear layer are shown on figure 7 for leading-edge thicknesses of 0.043 inch (figs. 7(a) and (b)) and 0.008 inch (figs. 7(c) and (d)). Of special significance is the low Mach number, low Reynolds number portion of these profiles, which exists near the wall. This portion of the shock-produced profiles will be referred to hereinafter as the low Reynolds number layer; defined in reference 12 as the streamtube passing between the vertex and the sonic point of the detached leading-edge shock wave. For a free-stream Mach number of 3.1, the thickness of this low Reynolds number layer is about 1.35 times the leading-edge thickness. The minimum Mach number within the low Reynolds number layer is 2.32, and the unit Reynolds number ratio $(u/\nu)_1$ to $(u/\nu)_\infty$ is 0.46.

The boundary-layer thickness is compared with the height of the low Reynolds number layer in figure 7. For truly inviscid flow the height of this layer would remain constant along the wall. Actually the boundary layer displaces the low Reynolds number layer outward by a distance equal to the displacement thickness of the boundary layer. The boundary-layer thickness is, therefore, compared in figure 7 with the displaced, as well as with the initial, height of the low Reynolds number layer.

The boundary-layer thickness (taken where $u/u_1 = 0.99$) was computed by the method of reference 11 (for the isothermal zero heat-transfer case) using an outer-edge Mach number of 2.32 and a unit Reynolds number ratio of 0.46. Apparently, from figures 7(a) to (c), the boundary layer develops substantially within the low Reynolds number layer up to the transition point. For the case shown in figure 7(d), which is the 0.008-inch leading edge at the lowest test value of the unit Reynolds number, a boundary-layer thickness based on free-stream conditions is also shown. The actual boundary-layer thickness in this case probably lies between the two distributions shown. For both distributions, nevertheless, the boundary layer grows through the low Reynolds number layer before reaching the transition point indicated by the cross. Boundary-layer developments at two intermediate unit Reynolds numbers for the 0.008-inch leading edge also were found to emerge from the low Reynolds number layer before reaching the observed transition point.

If the transition Reynolds number is assumed to remain unchanged when the leading edge is blunted as in reference 12, then the transition point for those instances where the boundary layer develops entirely within the low Reynolds number layer should be about 2.2 (1/0.46) times as far downstream for the blunted leading edge as for the sharp. The observed transition-location ratios for the 0.008- and 0.043-inch leading edges were between 2.17 and 1.8 for the three highest unit Reynolds numbers (figs. 4(a) to (c)) and 1.5 for the lowest (fig. 4(d)). For the lower unit Reynolds numbers, however, the transition points approach and finally reach the position where the reflected leading-edge shock strikes the model surface. This may account for the slightly smaller relative movement of transition in these cases. The fact that the boundary layer tends to grow up through the low Reynolds number layer as the unit Reynolds number is reduced may also partly account for the lower transition-point-location ratio.

The concept of immersing the entire laminar boundary layer within the low Reynolds number layer, however, may be unnecessary for the following reasons: (1) The unit Reynolds number increases slowly beyond the low Reynolds number portion of the shock-produced shear layer, and (2) the portion of the boundary layer sensitive to the stabilizing influence of the low Reynolds number layer may be relatively close to the surface or near the leading edge. The idea of the low Reynolds number layer, nevertheless, explains in substance the observed downstream movement of transition.

A portion of the decreases in transition Reynolds number with reductions in unit Reynolds number (for any given leading-edge thickness) reported in references 1, 2, and 8 can also be explained on the basis of a low Reynolds number layer at the surface. Thus, a comparison of figures 7(c) and (d) shows that when the laminar boundary layer emerges

from the low Reynolds number layer relatively near to the leading edge (low unit Reynolds number) the transition Reynolds number will be comparatively low, and vice versa.

Only transition delays produced by simple blunting of the leading edge have been discussed herein. For the case of the external bevel, where the Reynolds number change across the oblique shock would be considerably less than for the blunted edge, considerably more downstream movement of transition was observed. A table showing the computed Mach number and Reynolds number at the edge of the boundary layer and the experimentally observed ratio of transition-point locations for three leading-edge geometries at a unit Reynolds number of 3.5×10^5 per inch follows:

Leading edge	Mach number, M_1	Unit Reynolds number ratio, $\frac{(u/\nu)_1}{(u/\nu)_\infty}$	Transition-location ratio, $\frac{(x_t)_\infty}{(x_t)_1}$
Sharp, no external bevel	3.1	1.0	1.00
Sharp, 30° external bevel	2.69	.65	.42
Blunt, no external bevel	2.32	.46	.50

For the external bevel, therefore, larger gains in transition location than possible by simple leading-edge blunting were observed, notwithstanding the smaller Reynolds number reduction across the leading-edge shock. This suggests that appreciably greater gains resulting from improved leading-edge flow conditions or the establishment of pressure gradients conducive to stable laminar flow may be possible by careful design of the leading edge.

One factor ignored in the previous explanation for the transition delays is the favorable effect of the reduced boundary-layer outer-edge Mach number on the minimum critical Reynolds number for stability. (For the present tests this effect would approximately triple the minimum critical Reynolds number for the blunted leading edge and double it for the external bevel, if it were applicable in both cases. This estimate is based on values obtained from fig. 11 of ref. 13) using the Mach numbers listed in the preceding table.) If it may be assumed that an increase in the minimum critical Reynolds number results in a transition delay, then the assumption that the transition delay is entirely

due to the Reynolds number reduction within the shock-induced inviscid shear layer may require some modification.

While the simple Reynolds number reduction explanation suffices for most of the data presented in this report, an exception occurs for the external-beveled leading-edge model for which a transition delay greater than predicted was observed. For this case, it may be argued that the disturbance introduced into the boundary layer by the external-beveled leading edge was small compared with that produced by the blunted leading edges; and the stability theory of reference 13, which is based on small disturbances, hence could apply only to the external-beveled leading edge. Such an approach again suggests that important gains in transition delay may be realized by a careful shaping of the leading edge, not to mention reduction in leading-edge wave drag.

In the previous discussion of boundary-layer profiles shown in figure 6, decreases in outer-edge velocity were found to occur for the blunted leading edge and for the external bevel. These velocity decrements can be directly related to the total-pressure losses associated with the blunted leading edges or the oblique-shock formation due to the external bevel. Hence, in order to make a valid comparison between experimental and theoretical boundary-layer profiles, apparently the theoretical profiles must be based on the conditions at the boundary-layer outer edge rather than on the free-stream condition (these latter conditions were used in computing curve I in fig. 6.) Since no method is available for computing the laminar boundary layer developing through a shear layer, only the case of boundary-layer development in the relatively constant velocity region near the wall (as shown in fig. 7) will be considered. This restricts the problem more or less to the 0.008-, 0.043-inch, or the external-beveled leading edge.

Laminar-boundary-layer profiles, with the conditions given in the previous table assumed to prevail at the outer edge, were computed. Since no knowledge of the actual static-pressure gradients near the leading edge was available, the boundary layers were computed from the theory of reference 11 assuming a zero pressure variation along the surface. The profiles are plotted in figure 6 and are labeled II and III for the blunted and external-beveled leading edges, respectively. Because the distance from the leading edge to the boundary-layer survey station was shortened from 2.45 to 2.0 inches as the bluntness was increased from 0.0008 to 0.043 inch, curve II represents the boundary-layer profile at a distance of 2.0 inches and curves I and III, 2.45 inches from the leading edge.

The agreement between the free-stream Mach number and that predicted from the total-pressure losses across the leading-edge shock was very good, thus substantiating the shock-produced shear-layer velocity change predicted in reference 12. However, the experimental

points for the sharp leading edges generally lie above the computed curve, the discrepancy being largest for the high unit Reynolds numbers (thin boundary layers) and vanishing for the lowest (thick boundary layers). Considering the simplifications made in calculating the boundary layer within the shear layer, the agreement between the experimental and computed profiles appears reasonable.

Values of the laminar recovery factor based on conditions at the edge of the boundary layer rather than free-stream conditions may be computed for the 0.043-inch and the external-beveled leading edges. For the 0.043-inch leading edge with a measured free-stream recovery factor of 0.885 at an x of 2 inches (fig. 4), the new recovery factor based on conditions at the edge of the boundary layer ($M = 2.32$, $(u/\nu)_1/(u/\nu)_\infty = 0.46$) is found to be 0.851. For the external-beveled leading edge with a measured recovery factor of 0.868, the new recovery factor (based on the conditions $M = 2.69$, $(u/\nu)_1/(u/\nu)_\infty = 0.65$) is again found to be 0.851. Thus, the recovery factor near the leading edge has the proper laminar value when based on conditions at the edge of the boundary layer. No allowance has been made in this computation for heat transfer from the external to the internal surface for the external-beveled leading edge.

3882

Roughness Elements in Laminar Boundary Layer

In view of the preceding results, a brief test was conducted to determine what effect the leading-edge thickness would have on the roughness required to cause the transition from laminar to turbulent flow. Results that indicate the effectiveness of several single roughness elements in promoting transition at Mach 3.1 are given in reference 8. These results were obtained on a cylindrical model very similar to the one described in the present report, but having a leading edge of 0.006-inch thickness. The present results were obtained using a 0.001-inch leading edge; these will be compared with the referenced results in order to determine how the leading-edge thickness affects artificially induced transition.

A single roughness element made of a wire with a 0.052-inch diameter was placed at one of three positions, 1.25, 2.50, or 5.00 inches from the leading edge. Transition locations (designated x_t) were measured from the leading edge using the same peak-temperature criterion as in reference 8. These data are presented in figure 8 as a plot of transition position against unit Reynolds number, with and without roughness.

The general behavior of transition with single-roughness elements may be summarized from figure 8. Reductions in unit Reynolds number cause transition to move downstream much as it would without any roughness present until it reaches the roughness element. Further reductions in u_∞/ν_∞ show a tendency for transition to remain at the element and

to depart from it only after rather large reductions have taken place. Transition then proceeds downstream at an increasing rate as u_∞/ν_∞ is reduced still further. Transition may also be displaced upstream or downstream by moving the roughness element in like manner, provided, of course, that transition is always downstream of the element.

Although the data for the element at a distance x_k of 5 inches show transition to be somewhat downstream of the zero-roughness transition position for values of $u_\infty/\nu_\infty > 4\times10^5$, in the analysis which follows transition will be assumed to occur at the zero-roughness position for these values. The reason this assumption was made follows from a certain ambiguity between the temperature peak caused by transition and that caused by the roughness element. (A further discussion of this point appears on p. 12 of ref. 8.)

A correlation of the roughness data is given in figure 9 in terms of the transition Reynolds number ratio $Re_t/Re_{t,0}$ and the roughness parameter k/δ_k^*. These parameters are developed in reference 14 to correlate low-speed roughness results and are used in reference 8 to correlate roughness data at Mach 3.1. Also included for comparison are curves from reference 8 for the same size roughness element at the same position on the model, but for a 0.006-inch leading edge. The correlation curve for the low-speed data of reference 14 is shown at the left.

In applying the roughness correlation of reference 14, it is necessary to determine whether the leading-edge phenomena noted in the previous section affect the calculation of the various parameters involved. Since both the numerator and denominator in the parameter $Re_t/Re_{t,0}$ are always chosen for the same leading edge, any distinction between a thick and thin leading edge is not necessary.

The same reasoning does not apply, however, if the change in Reynolds number caused by the roughness element must be considered. Thus, if the unit Reynolds number behind the element is reduced by the shock off the element (analogous to the reductions caused by a curved leading-edge shock), then a reduction in the parameter $Re_t/Re_{t,0}$ will result. Such a reduction would also serve to bring the supersonic roughness correlation of reference 8 and the present report into better agreement with the subsonic correlation. In view of the questionable nature of such a calculation, however, the roughness-element shock has not been considered in figure 9.

For the parameter k/δ_k^*, it will generally be necessary to calculate δ_k^* at a reduced Mach number and unit Reynolds number if the leading edge is blunted. In the present instance, the change in δ_k^*, assuming

the reduced Mach number and unit Reynolds number given previously, is approximately a 1-percent increase over δ_k^* calculated for the free stream. This difference has been neglected in representing the results obtained from reference 8 in figure 9 of the present report.

Because of the difference between the trends of the results for the 0.001- and 0.006-inch leading edges in figure 9, it is difficult to make a comparison. If an envelope line is drawn through the left extremity of the data for the 0.001-inch leading edge and another, similarly, for the 0.006-inch edge, these may be considered lines along which the roughness elements had their maximum effect on reducing the transition Reynolds number ratio. Using these lines as a basis of comparison, figure 9 shows that a roughness-parameter increase of about 1.4 times is required when the leading-edge thickness is increased from 0.001 to 0.006 inch. Compared with the low-speed curve of reference 15, the roughness requirements for the 0.001- and 0.006-inch leading edges at Mach 3.1 are over four and six times the low-speed values, respectively.

When a detailed comparison is made between the data for the 0.001- and 0.006-inch leading edges at a given value of x_k, the conclusions drawn in the former comparisons are not always true. In fact, there are situations where the thin leading edge shows greater stability with respect to the roughness than the blunted. This occurs when transition is fairly close behind the element. When transition is far downstream of the element, the blunted-leading-edge model exhibits the greater stability, as mentioned in the previous paragraph.

Surface-Heat Condition Effects

An analytical method is given in reference 2 for calculating the effect of surface-heat conduction on the temperature distributions measured at the surface of a flat plate insulated on one side. The results obtained with this method were compared with the experimental temperature distribution obtained on the stainless-steel cylindrical shell tested in reference 2. The comparison showed that a small but significant portion of the temperature rise in the laminar-boundary-layer region was caused by heat conduction along the model surface from the high-temperature transition region. In order to investigate further the relative importance of surface-heat-conduction effects, two additional tests have been made using surface materials having much smaller and much greater conductivities than the stainless-steel shell.

Conduction effects are functions not only of the surface conductivity k_s, but depend also on the surface thickness t, the local-heat-transfer coefficient h, and the distance from the leading edge x_f

that the flow can be considered laminar. These quantities can be summarized by the conduction parameter K, where

$$K = \frac{hx_f^2}{k_s t}\sqrt{\frac{x}{x_f}}$$

(This parameter is derived in ref. 2, where it is written in different but equivalent terms.) The heat-transfer coefficient h is defined by equation (52), reference 11, assuming the surface-temperature distribution to be expressible in terms of a simple power relation

$$\frac{T_w - T_{ad}}{T_\infty} \propto \left(\frac{x}{x_f}\right)^n$$

Values of thermal conductivity, shell thickness, and K for the models tested are tabulated below:

Model shell material	Conductivity Btu/(hr)(ft)(°F)	Shell thickness, in.	Conduction parameter, K
Fiberglas plastic laminate	~0.1	0.09	1820 to 4260
18-8 Stainless steel	9.4	.032	50.7 to 103.2
Pure copper	223	.03	1.68 to 5.22

Conduction parameters are thus seen to range from about 30 times smaller to 30 times larger than that of the stainless-steel shell reported in reference 2.

Typical recovery-factor distributions obtained for the three cylinder models are presented in figure 10 for a unit Reynolds number of about 3.5×10^5 per inch. A comparison of the distributions for the Fiberglas-plastic and stainless-steel models shows an upstream displacement of the transition point (temperature peak) of about 1/2 inch. This displacement occurs despite the fact that the leading edge of the Fiberglas-plastic model is more blunt and, hence, is very likely caused by the increased surface roughness noted earlier for this model. The copper surface on the other hand, has a more gradual temperature variation, indicating a definite smoothing out of the temperature profile as a result of the large surface conduction. Temperature peaks became smaller and are displaced downstream slightly with increased conduction. This displacement is believed to be caused by an increasing conduction

rather than an actual shift in transition point. Instrumentation difficulties probably are responsible for the over-all recovery-factor drop on the copper model, but they do not in any way affect the location of transition.

A calculation of the theoretical surface-temperature distribution θ against ξ using the method given in reference 2 is presented in figure 11, together with the experimental distributions. The variables θ and ξ are defined as

$$\theta = \frac{T_w - T_{ad}}{T_f - T_{ad}}$$

$$\xi = \frac{x}{x_f}$$

where T_w is the variable surface temperature, T_{ad} is the adiabatic surface temperature, and T_f is the final value of the measured surface temperature at the downstream extremity of the laminar run. The term x_f is the value of x at which T_f occurs. The conduction parameters which were previously tabulated are indicated in figure 11.

A comparison of the experimental and theoretical temperature distributions for the Fiberglas plastic sleeve (fig. 11(a)) reveals large discrepancies. Not only are the experimental distributions more gradual, but the trend for increasing K is reversed from theory. The results for the stainless-steel model (fig. 11(b) also fig. 8 of ref. 2) show a smaller discrepancy between experiment and theory; however, the difference between the stainless-steel and Fiberglas plastic experimental distributions are insignificant. Lastly, the results for the copper sleeve (fig. 11(c)) show considerably better agreement than for the steel, and the distributions follow in the proper order for increasing K.

These results show that when conduction effects are large, surface temperature will be primarily determined by conduction and only secondarily by convection in the laminar boundary layer; and when conduction is small, the convection effects will predominate over the conduction. Hence, if the actual heat-transfer rate is not the laminar-flat-plate value assumed in the computations, but is somewhat modified by the impending transition to turbulent flow, then a larger error in the resulting temperature distribution will occur when the conductivity is low rather than when it is high. These observations suggest that the schlieren photographs and the present temperature-measurement technique do not define a region in which the laminar boundary layer behaves according to theory, even for a zero pressure gradient.

Effect of Stream Total Temperature

The temperature distribution and transition position for a given leading-edge configuration has, until now, been assumed to be a function of the unit Reynolds number rather than of the pressure or temperature of the stream. The correctness of this assumption has been investigated in this report for the case of the sharpest-leading-edge model having a 5° internal bevel by raising the tunnel total temperature from about 52° to 176° F and making suitable increases in total pressure to maintain constant values of unit Reynolds number.

Recovery-factor distributions obtained at a unit Reynolds number of 3.5×10^5 per inch for total temperatures of 52° and 176° F are shown in figure 12. These curves show close agreement as to the position of the transition point but differ somewhat in the absolute value of the laminar and turbulent recovery factors. The close agreement regarding transition position was also noted at other values of unit Reynolds number, and shows that this number is the more significant parameter controlling transition location, rather than stream temperature or pressure.

The differences in the laminar and turbulent recovery-factor levels at these two temperatures can be accounted for in part by considering Prandtl number variations resulting from the differences in surface temperatures. The measured and computed values of the recovery factor based on the Prandtl number evaluated at the wall are listed in the following table.

T_o, $^{\circ}$F	Laminar		Turbulent	
	176	52	176	52
η (measured)	0.856	0.860	0.883	0.888
T_w, $^{\circ}$F	116	6	128	13.5
Pr	0.703	0.719	0.702	0.711
η (computed)	0.839	0.848	0.889	0 893

Computed values for the laminar and turbulent recovery factors are based on the square root and cube root Prandtl number approximation, respectively.

Although the measured trend in recovery factor is apparently prescribed by the wall temperature level T_w, the exact value of η is in error. The difference between the measured and computed values are two to three times larger for the laminar then for the turbulent recovery

factors. Radiation from the tunnel and room, or heat conduction from the inside to the outside of the model, may be responsible for these effects.

CONCLUDING REMARKS

The large observed downstream movement of transition when the sharp leading edge of a hollow cylindrical model is slightly blunted has been associated with the formation of a shock-produced shear layer adjacent to the model surface. Ordinarily, the layer is formed by the large total-pressure losses occurring in the strongly curved portion of the detached shock resulting from the blunted leading edge. These pressure losses cause the unit Reynolds number and Mach number in the region near the wall to be substantially less than their free-stream values. It is in this region that the boundary layer develops. In addition to the direct evidence of transition delay caused by blunting the leading edge, the following observations tend to confirm this proposed explanation:

(1) The delay in transition when a curved shock was placed ahead of a sharp leading edge

(2) The increases in free-stream laminar recovery factor with increasing leading-edge bluntness which were reduced to a common value based on local conditions

(3) The low measured velocity near the outer edge of the laminar boundary layer

Larger delays in transition than produced by blunting were obtained on an external-beveled leading edge, probably as the result of improved flow conditions at the leading edge.

A simplified comparison of the effect of roughness on transition with and without leading-edge blunting can be made if only the data yielding the maximum effect of roughness on transition are considered. In this case, increasing the leading-edge thickness has a favorable effect on the ability of a laminar boundary layer to withstand disturbances such as single-roughness elements. In terms of the roughness parameter (element height to displacement thickness k/δ_k^*), 1.4 times the roughness is required to produce a given change in the transition Reynolds number ratio for a 0.006-inch leading edge than for a 0.001-inch edge. A more detailed examination of the results reveals exceptions to these general conclusions which in some cases actually reverse these trends.

In the comparison of the copper model with the stainless-steel model, increasing the effective conductivity 30 times produced very significant changes in the observed temperature distribution; decreasing it 30 times produced almost imperceptible changes.

The dependence of transition-point location on the Reynolds number of the stream, rather than on the pressure or temperature exclusively, was established by varying the inlet pressure and temperature independently.

GENERAL REMARKS

Based on the preceding conclusions and observations made in the course of these tests, it is suggested that

(1) A conical body would be a more ideal test shape than a cylinder. The use of a cone would eliminate irregularities in the temperature distributions due to internal flow conditions and would alleviate leading-edge fabrication and measuring difficulties. Tests on a conical body furthermore would serve to check the extension of the analysis of Moeckel to three-dimensional bodies.

(2) A more extensive investigation of various other leading-edge shapes should be undertaken to get a better insight into the mechanisms involved and to determine what limits in optimizing transition delay are possible.

Lewis Flight Propulsion Laboratory
National Advisory Committee for Aeronautics
Cleveland, Ohio, December 15, 1955

REFERENCES

1. Brinich, Paul F., and Diaconis, Nick S.: Boundary-Layer Development and Skin Friction at Mach Number 3.05. NACA TN 2742, 1952.

2. Brinich, Paul F.: A Study of Boundary-Layer Transition and Surface Temperature Distributions at Mach 3.12. NACA TN 3509, 1955.

3. Dunning, Robert W., and Ulmann, Edward F.: Effects of Sweep and Angle of Attack on Boundary-Layer Transition on Wings at Mach Number 4.04. NACA TN 3473, 1955.

4. Lange, A. H., and Lee, R. E.: Note on Boundary-Layer Transition in Supersonic Flow. Jour. Aero. Sci., vol. 21, no. 1, Jan. 1954, p. 58.

5. Lange, A. H., and Lee, R. E.: Further Comments on "Note on Boundary-Layer Transition in Supersonic Flow." Jour. Aero. Sci., vol. 22, no. 4, Apr. 1955, p. 282.

6. Sternberg, Joseph: The Transition from a Turbulent to a Laminar Boundary Layer. Rep. 906, Ballistic Res. Labs., Aberdeen Proving Ground, May 1954.

7. Bradfield, W. S., DeCoursin, D. G., and Blumer, C. B.: The Effect of Leading-Edge Bluntness on a Laminar Supersonic Boundary Layer. Jour. Aero..Sci., vol. 21, no. 6, June 1954, pp. 373-382.

8. Brinich, Paul F.: Boundary-Layer Transition at Mach 3.12 with and without Single Roughness Elements. NACA TN 3267, 1954.

9. Evvard, J. C., Tucker, M., and Burgess, W. C., Jr.: Statistical Study of Transition-Point Fluctuations in Supersonic Flow. NACA TN 3100, 1954.

10. Ross, Albert O.: Determination of Boundary-Layer Transition Reynolds Numbers by Surface-Temperature Measurement of a 10° Cone in Various Supersonic Wind Tunnels. NACA TN 3020, 1953.

11. Chapman, Dean R., and Rubesin, Morris N.: Temperature and Velocity Profiles in the Compressible Laminar Boundary Layer with Arbitrary Distribution of Surface Temperature. Jour. Aero. Sci., vol. 16, no. 9, Sept. 1949, pp. 547-565.

12. Moeckel, W.: Some Effects of Bluntness on Boundary-Layer Transition and Heat Transfer at Supersonic Speeds. NACA TN 3653, 1956.

13. Van Driest, E. R.: Calculation of the Stability of the Laminar Boundary Layer in a Compressible Fluid on a Flat Plate with Heat Transfer. Jour. Aero. Sci., vol. 19, no. 12, Dec. 1952, pp. 801-812.

14. Dryden, Hugh L.: Review of Published Data on the Effect of Roughness on Transition from Laminar to Turbulent Flow. Jour. Aero. Sci., vol. 20, no. 7, July 1953, pp. 477-482.

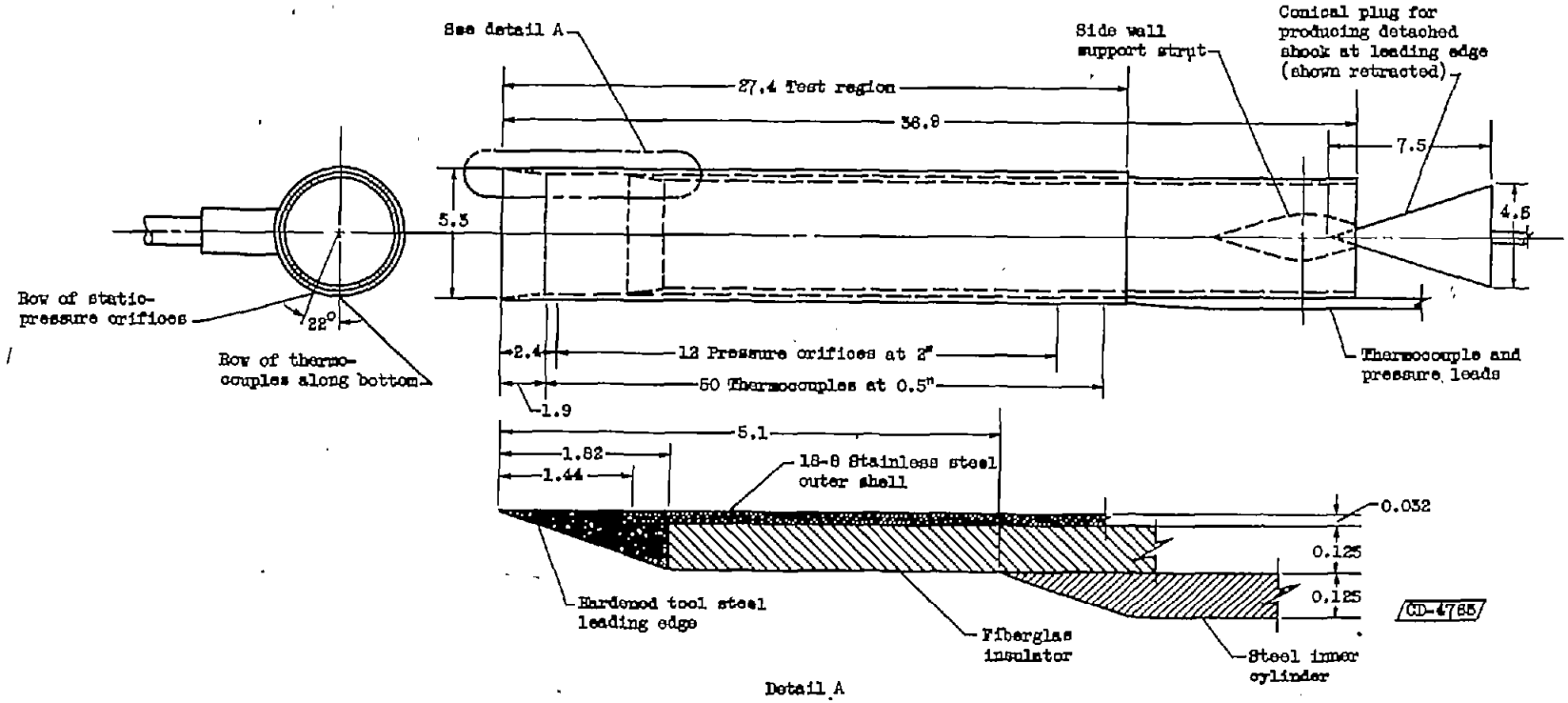

Figure 1. - Stainless-steel cylinder. (All dimensions in inches.)

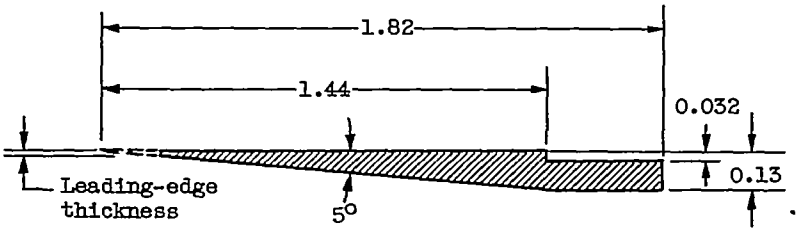

(a) 5° Internal bevel. Leading-edge thickness, 0.0008, 0.0028, 0.005, 0.008, 0.016, or 0.043 inch.

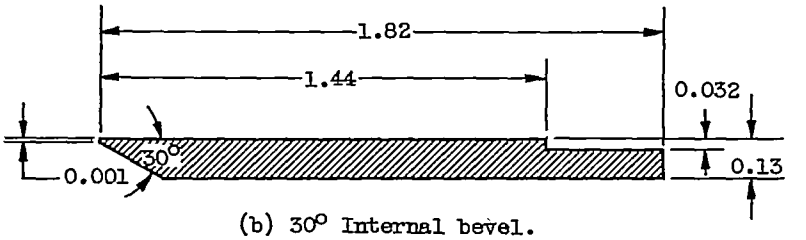

(b) 30° Internal bevel.

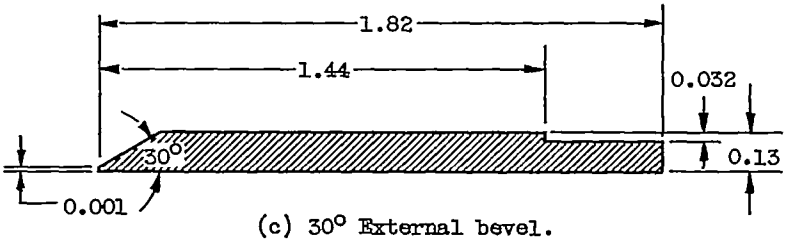

(c) 30° External bevel.

CD-4766

Figure 2. - Various leading-edge sections for stainless-steel and copper cylinders. (Dimensions are in inches.)

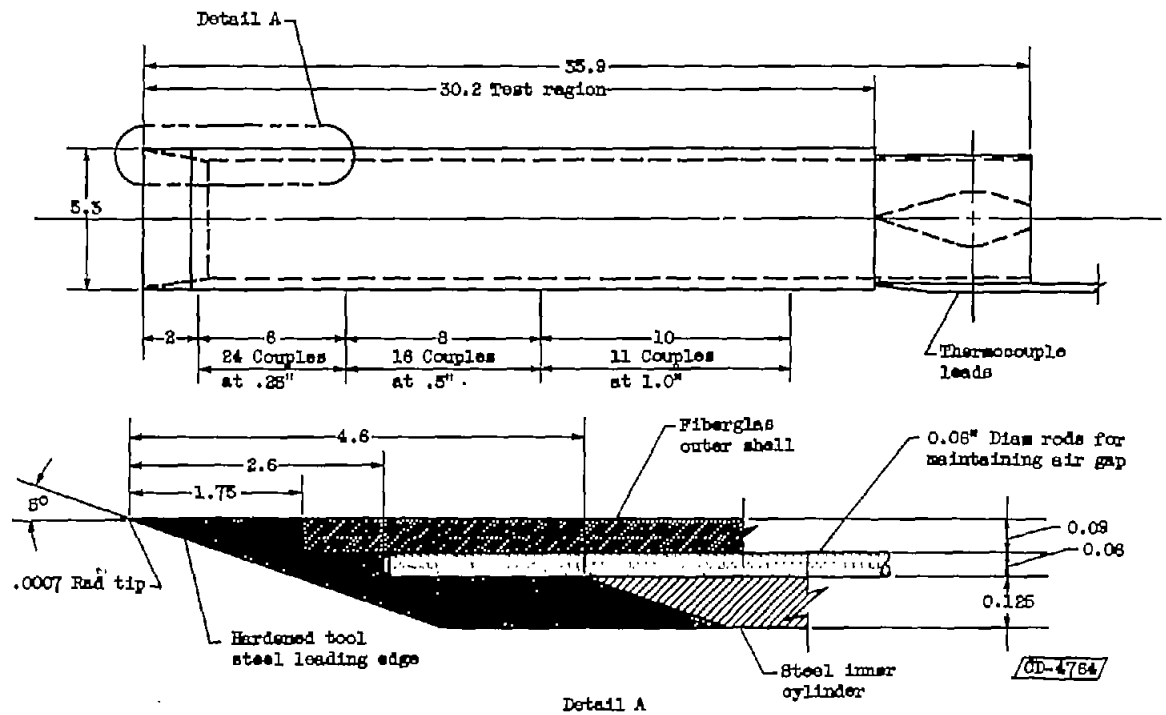

Figure 3. - Fiberglas cylinder model.

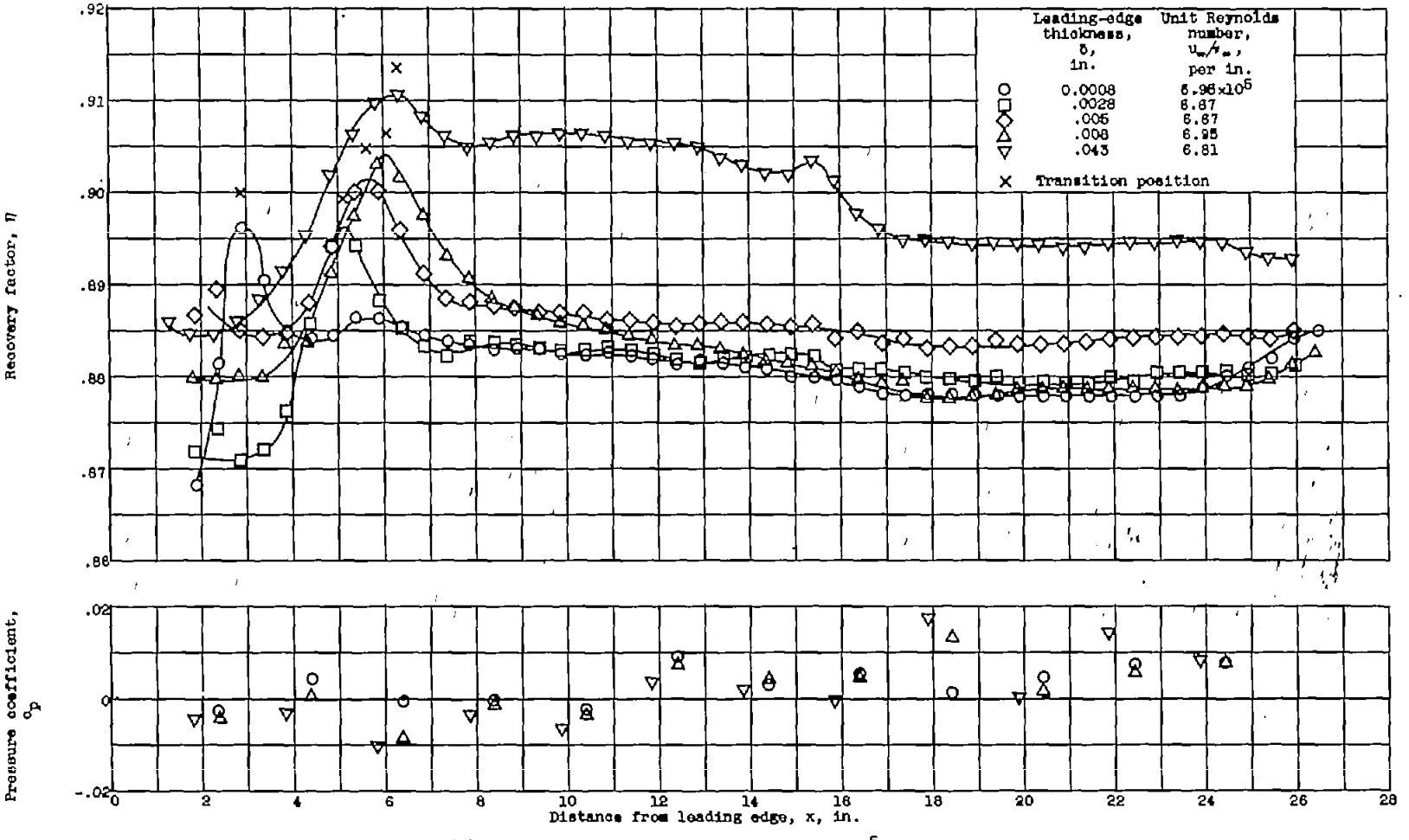

(a) Unit Reynolds number, approximately 6.8×10^5 per inch.

Figure 4. - Recovery-factor and pressure-coefficient distributions for various leading-edge thicknesses.

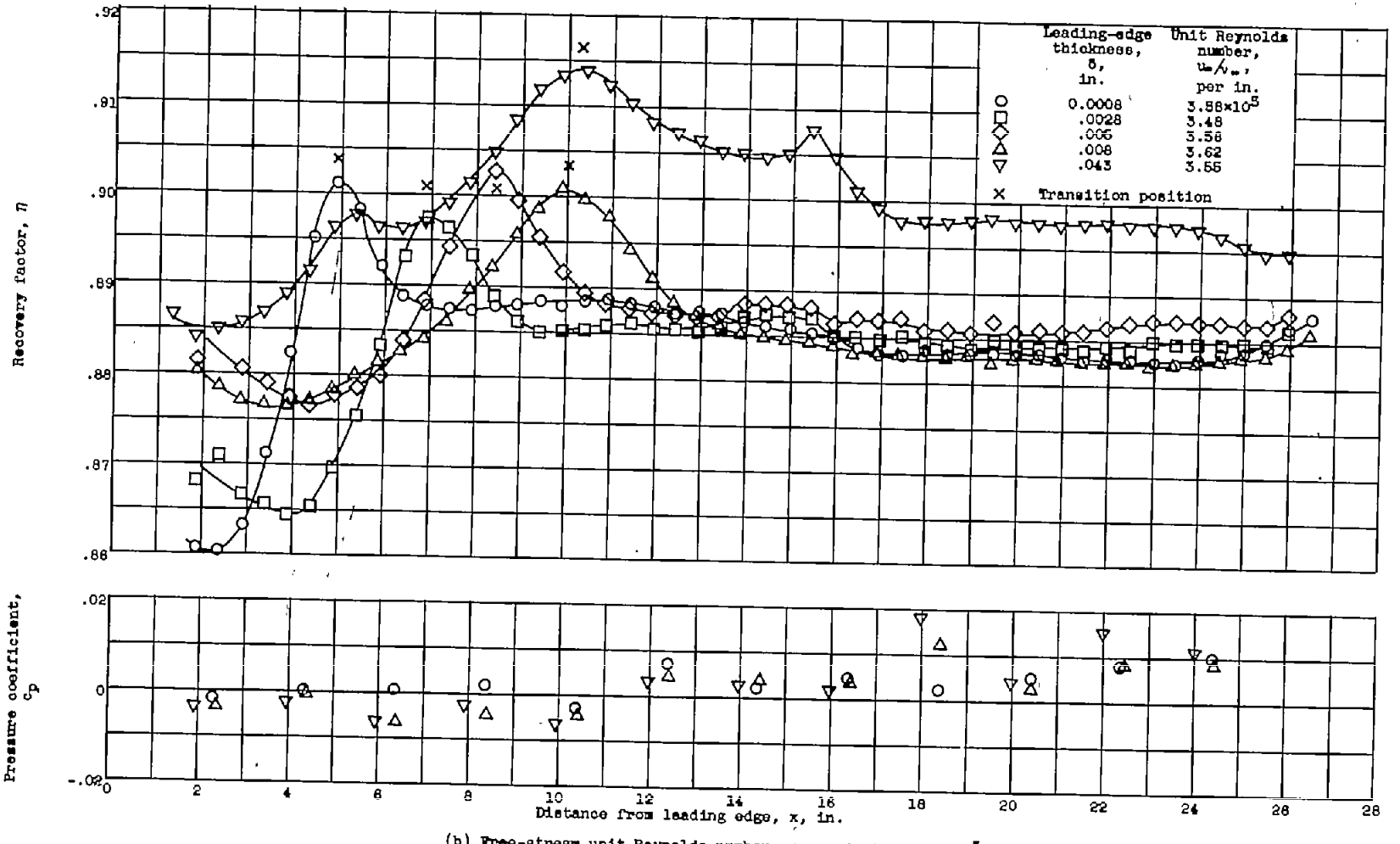

(b) Free-stream unit Reynolds number, approximately 3.5×10^5 per inch.

Figure 4. - Continued. Recovery-factor and pressure-coefficient distributions for various leading-edge thicknesses.

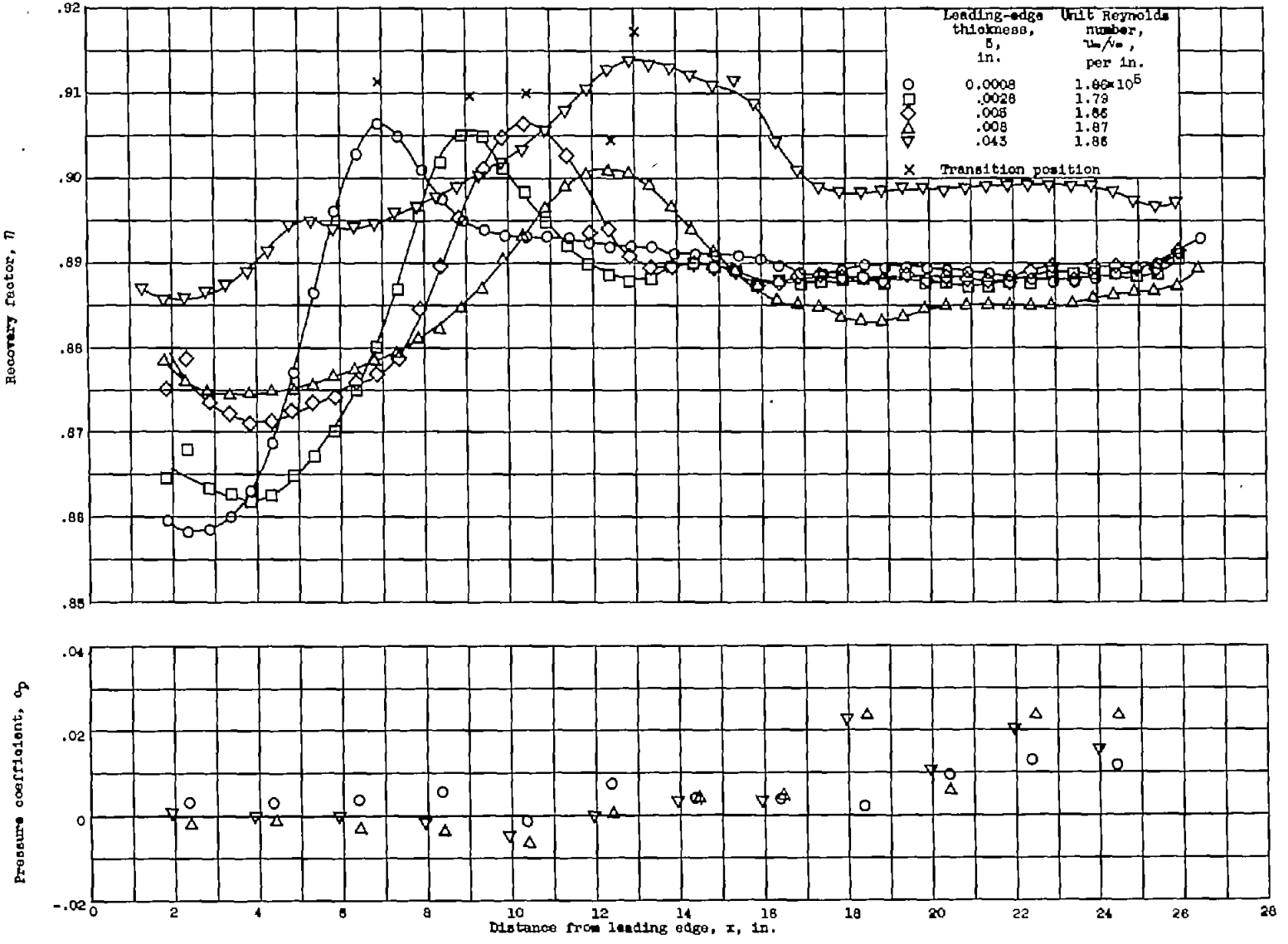

(c) Unit Reynolds number, approximately 1.86×10^5 per inch.

Figure 4. - Continued. Recovery-factor and pressure-coefficient distributions for various leading-edge thicknesses.

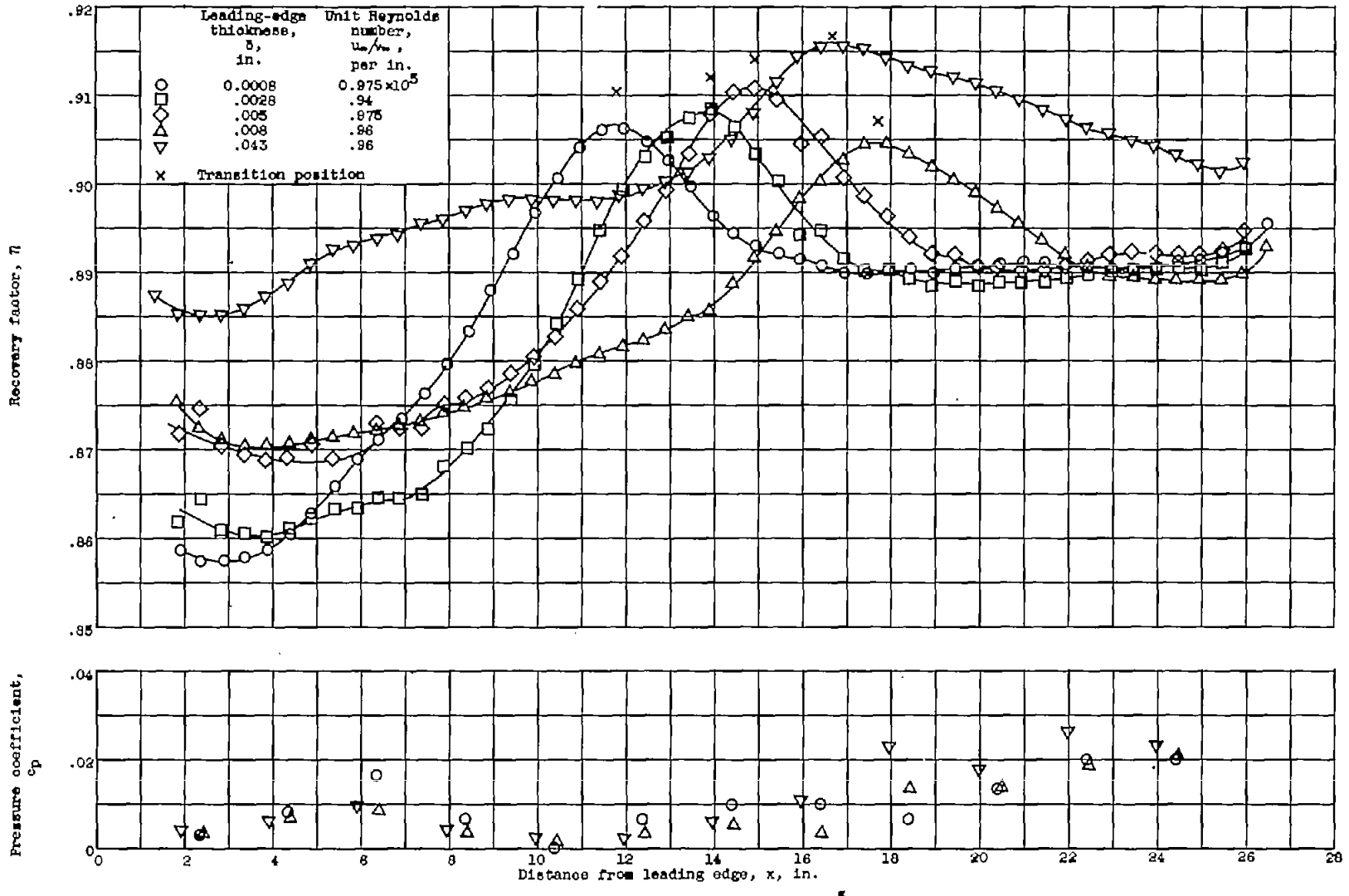

(d) Unit Reynolds number, approximately 0.98×10^5 per inch.

Figure 4. - Concluded. Recovery-factor and pressure-coefficient distributions for various leading-edge thicknesses.

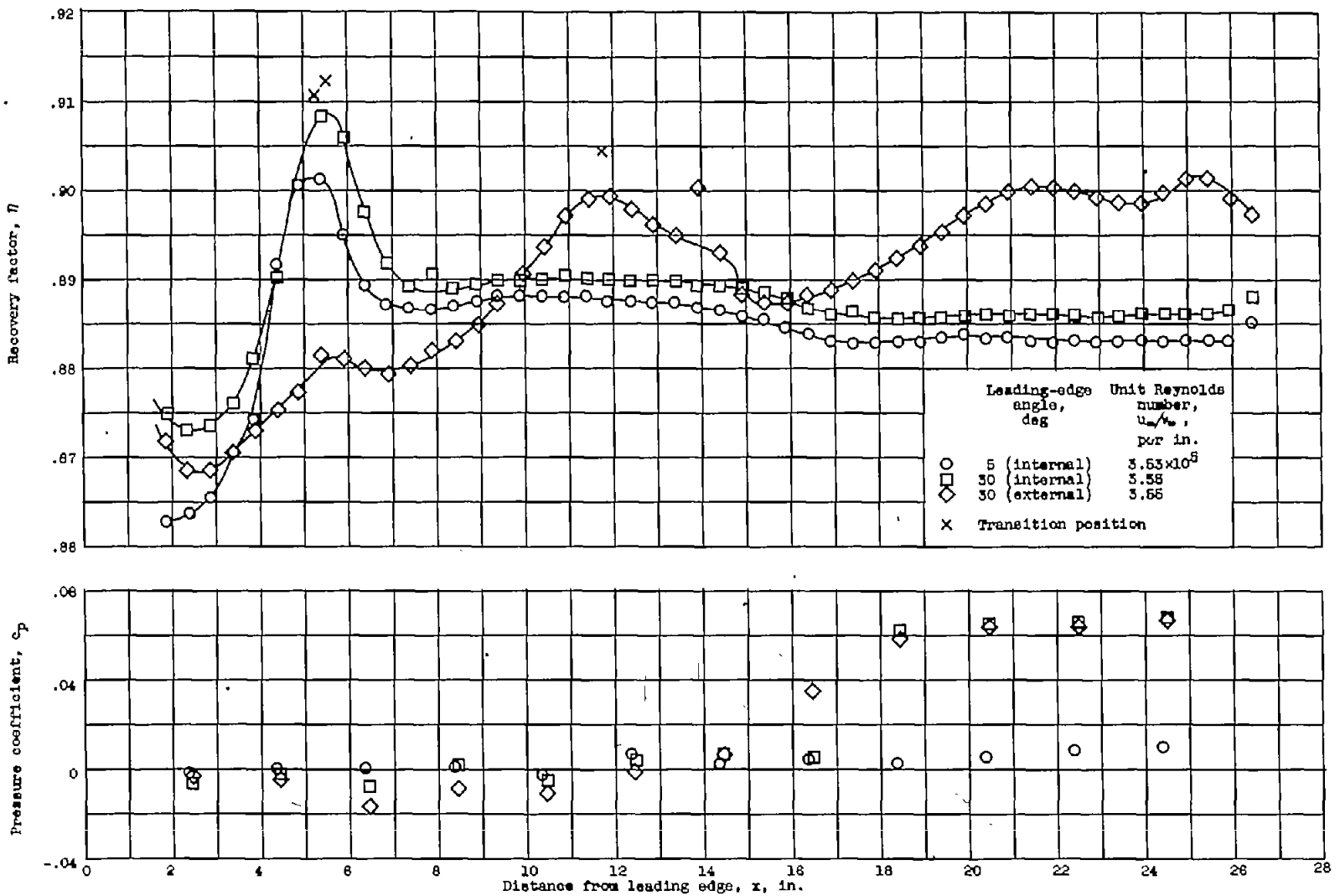

Figure 5. - Recovery-factor and pressure-coefficient distributions for three leading-edge angles. Free-stream Reynolds number, 3.5×10^5 per inch; leading-edge thickness, 0.001 inch.

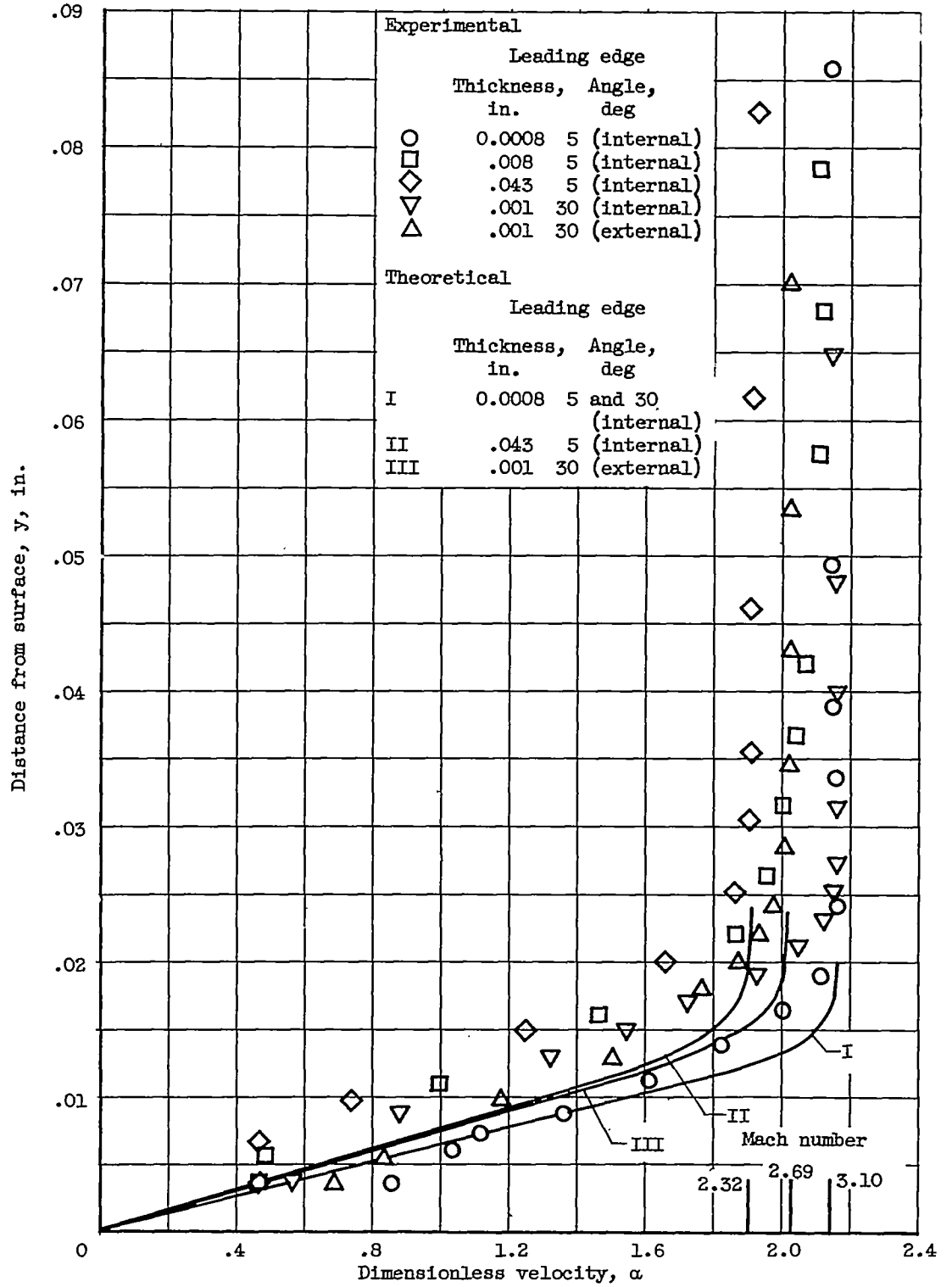

(a) Unit Reynolds number, 6.8×10^5 per inch.

Figure 6. - Effect of leading edge on boundary-layer profiles.

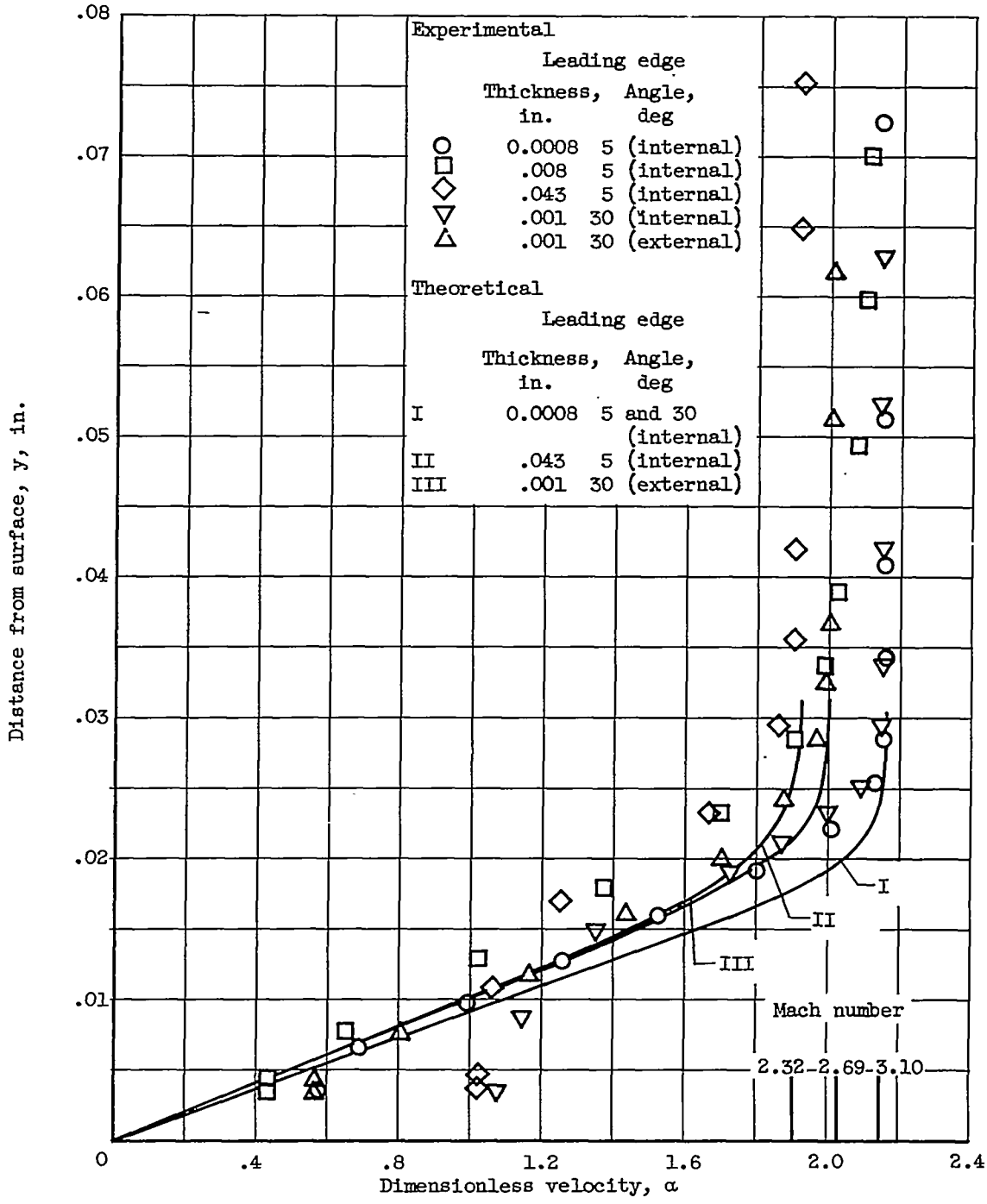

(b) Unit Reynolds number, 3.58×10^5 per inch.

Figure 6. - Continued. Effect of leading edge on boundary-layer profiles.

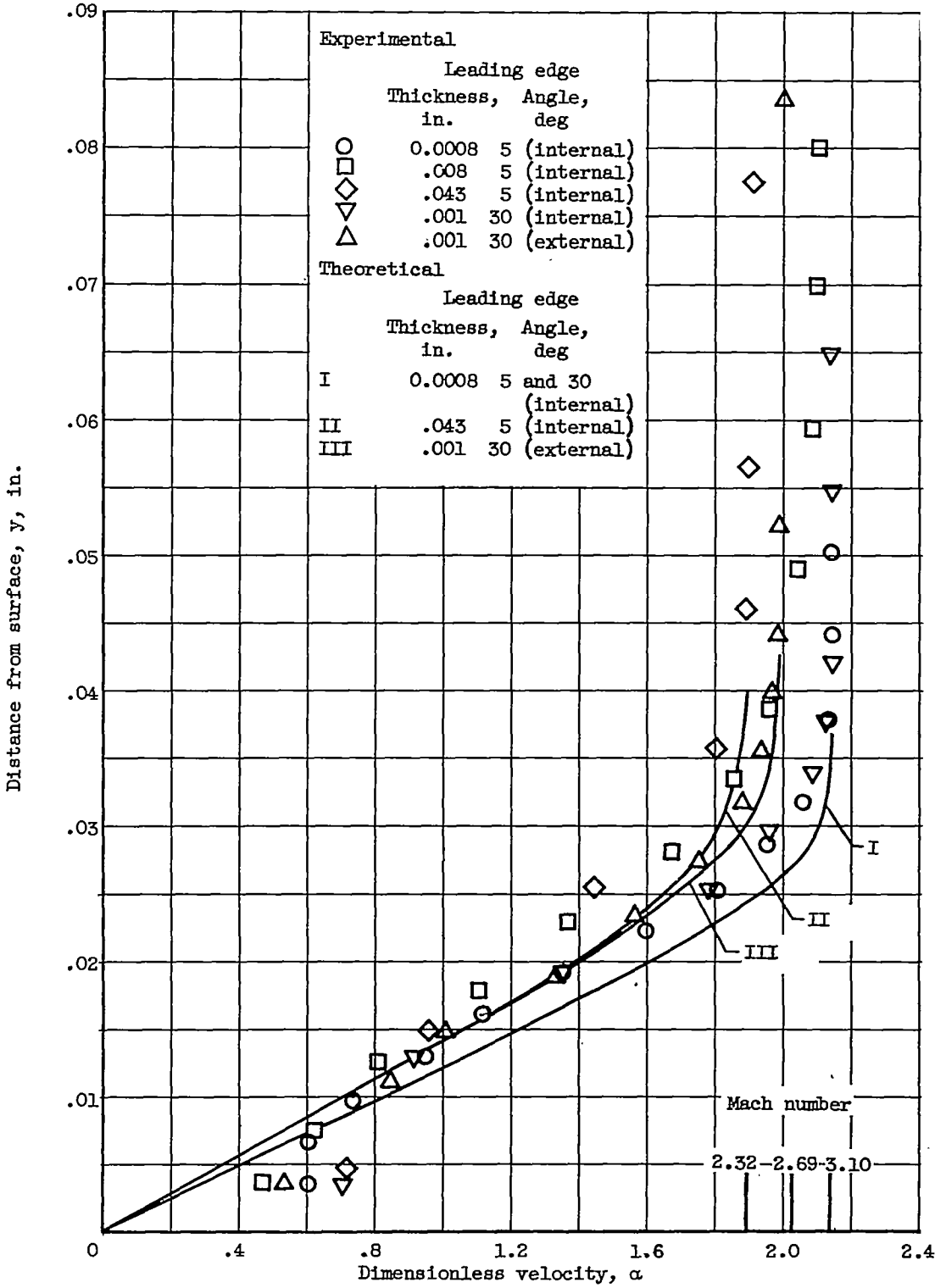

(c) Unit Reynolds number, 1.84×10^5 per inch.

Figure 6. - Continued. Effect of leading edge on boundary-layer profiles.

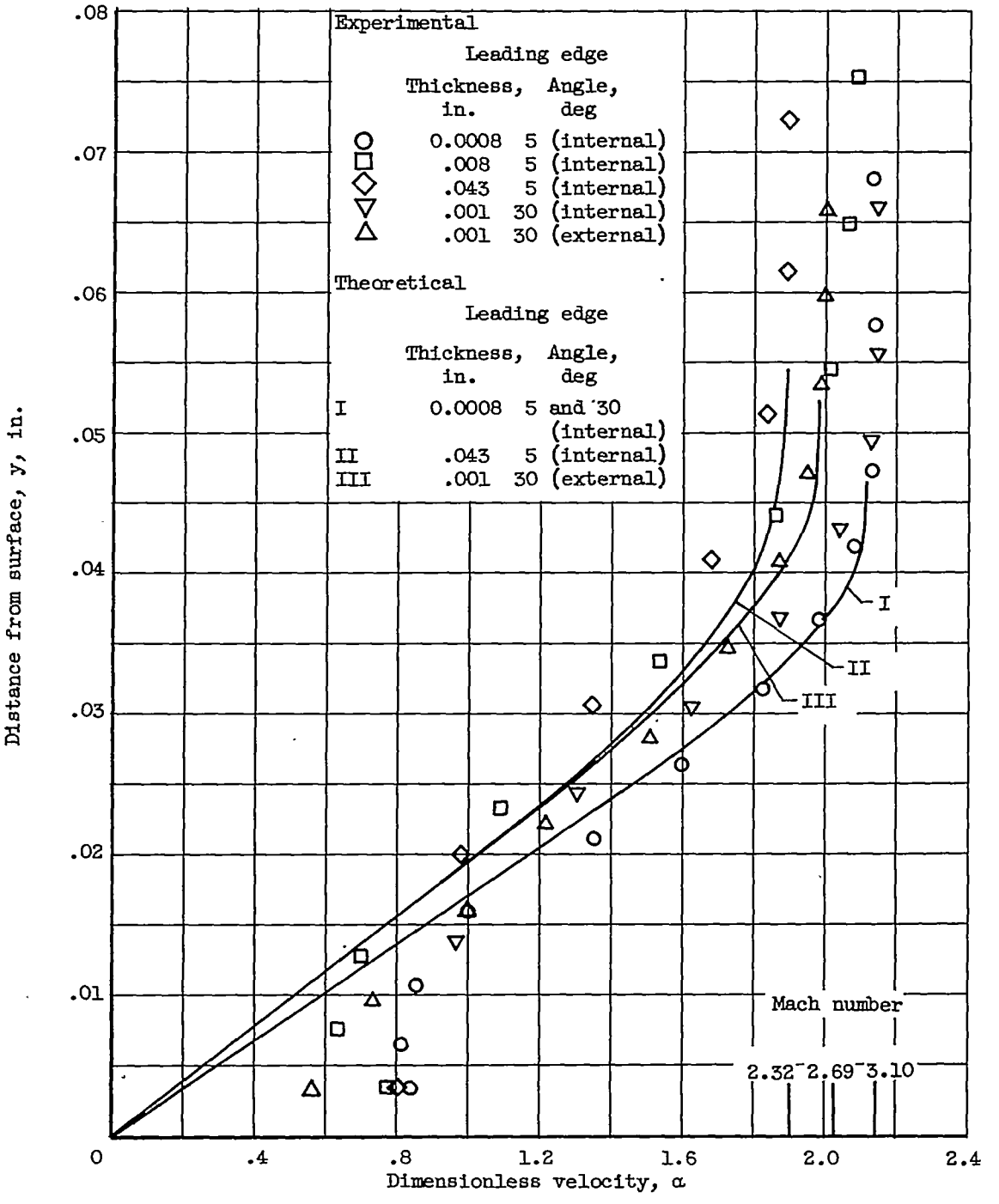

(d) Unit Reynolds number, 0.97×10^5 per inch.

Figure 6. - Concluded. Effect of leading edge on boundary-layer profiles.

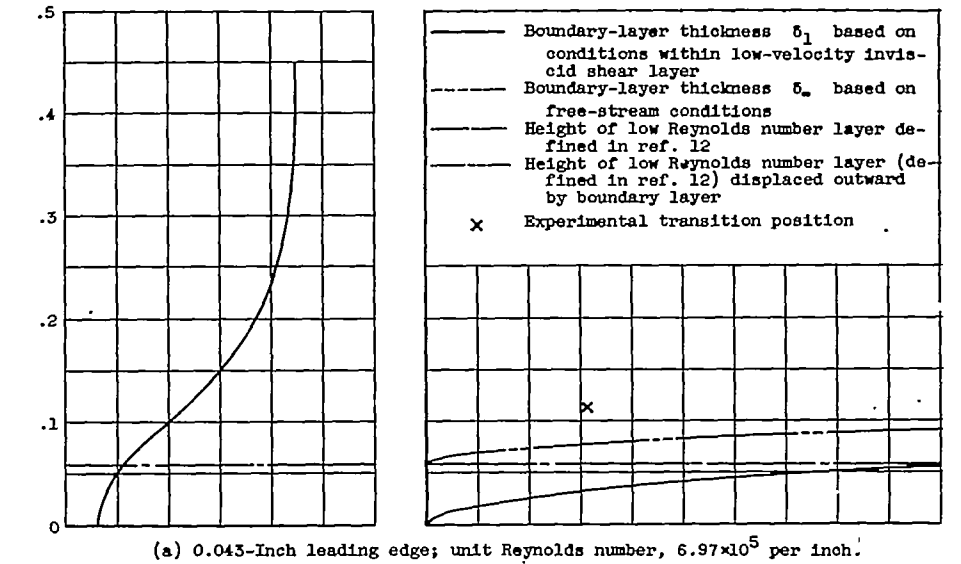

(a) 0.043-Inch leading edge; unit Reynolds number, 6.97×10^5 per inch.

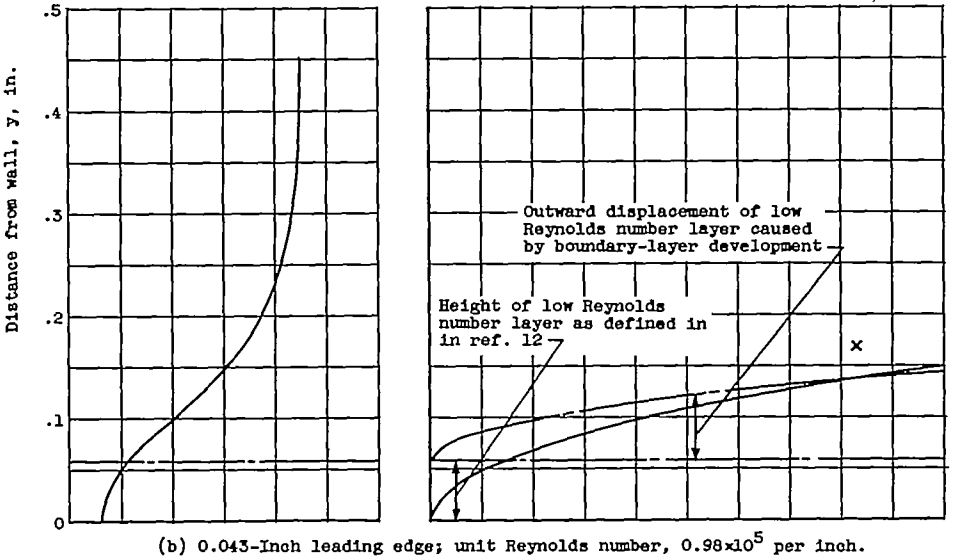

(b) 0.043-Inch leading edge; unit Reynolds number, 0.98×10^5 per inch.

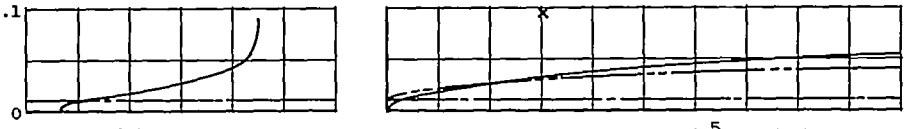

(c) 0.008-Inch leading edge; unit Reynolds number, 6.97×10^5 per inch.

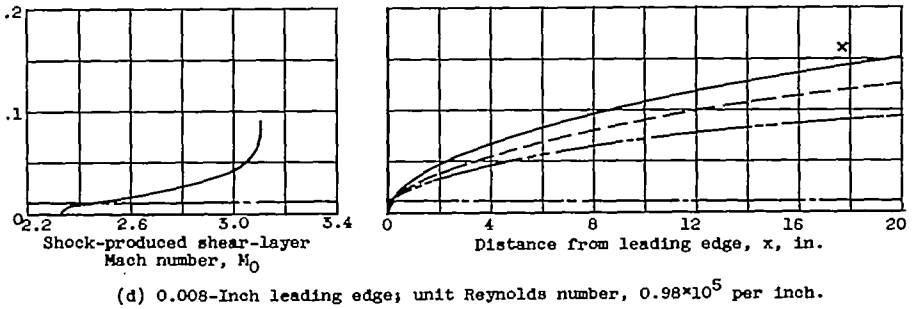

(d) 0.008-Inch leading edge; unit Reynolds number, 0.98×10^5 per inch.

Figure 7. - Boundary-layer development in presence of shock-produced shear layer.

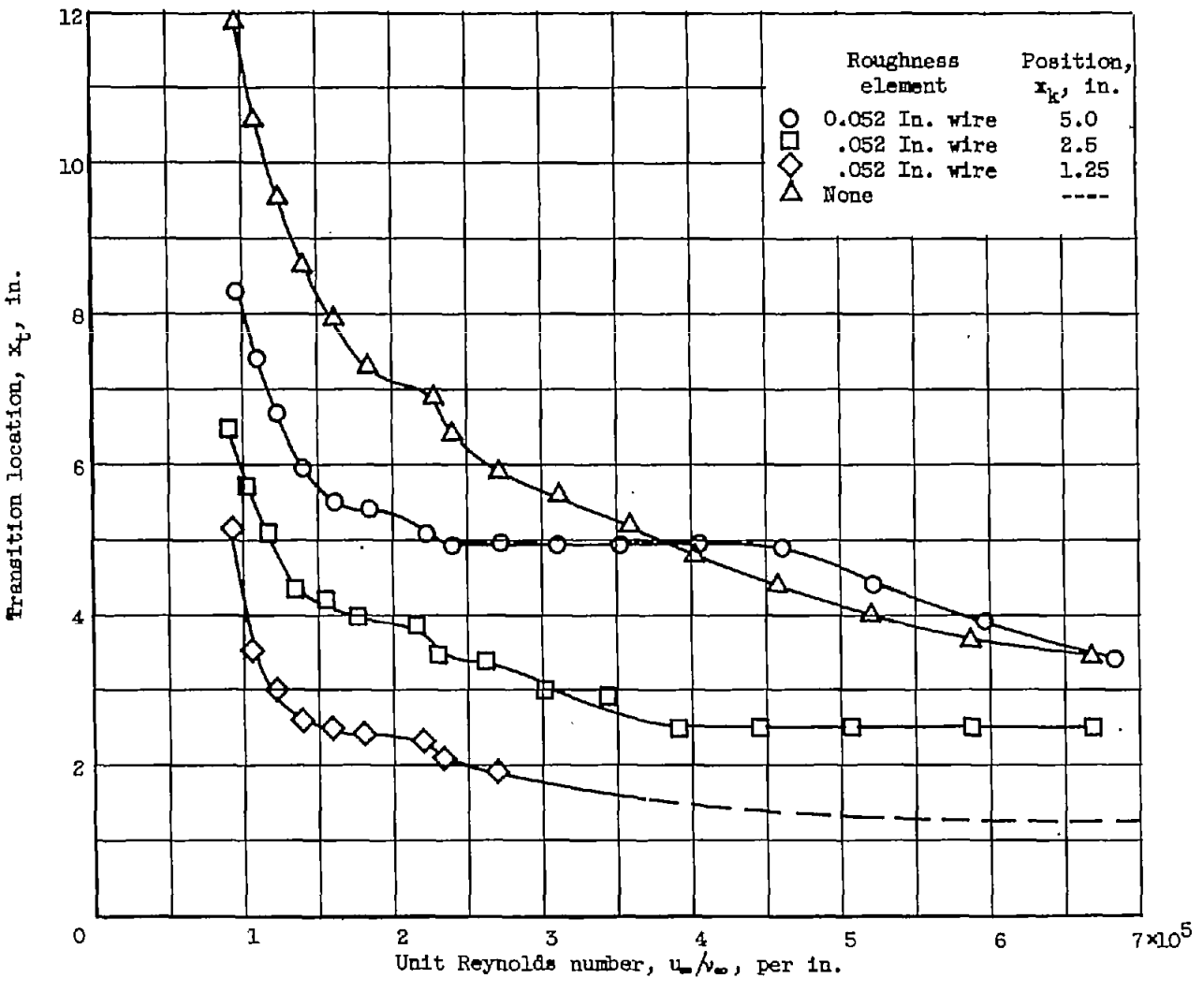

Figure 8. - Effect of free-stream Reynolds number and roughness-element position on transition.

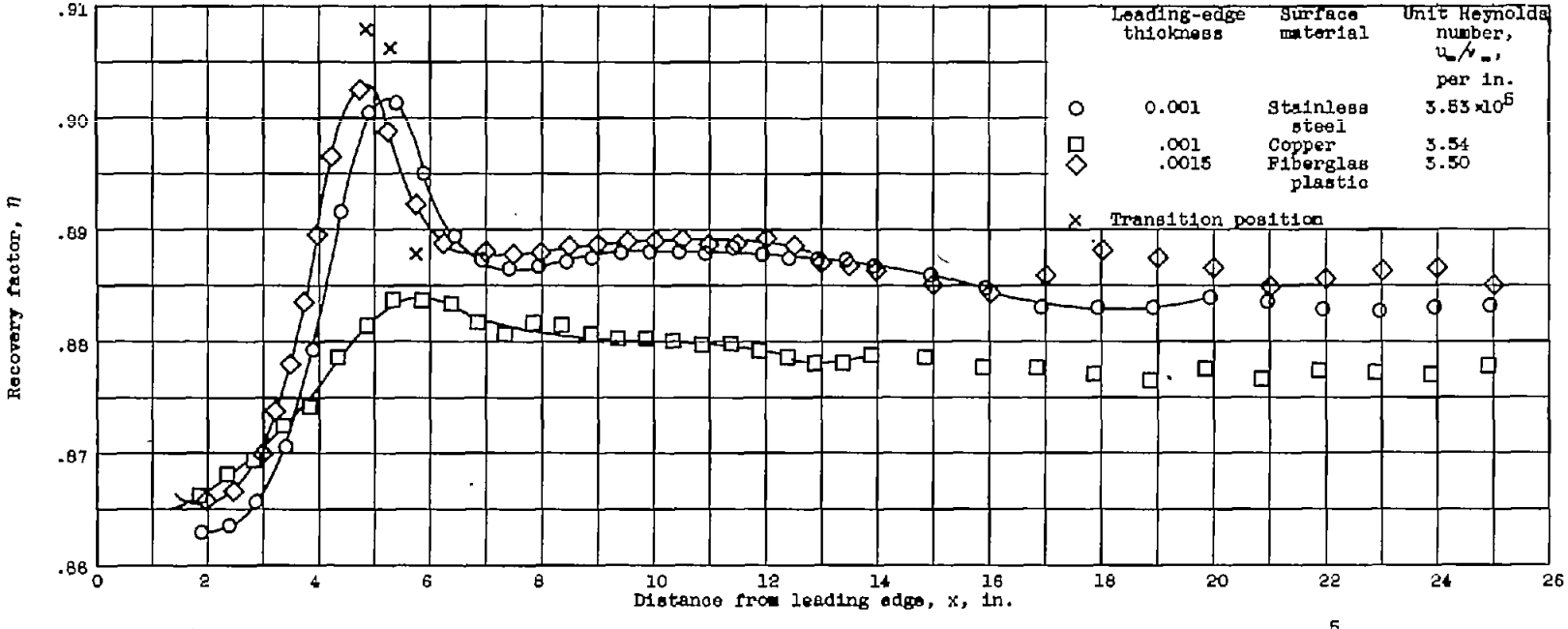

Figure 10. - Recovery-factor distributions for surfaces of varying conductivity. Unit Reynolds number, 3.5×10^6 per inch; internal leading-edge angle, 5°.

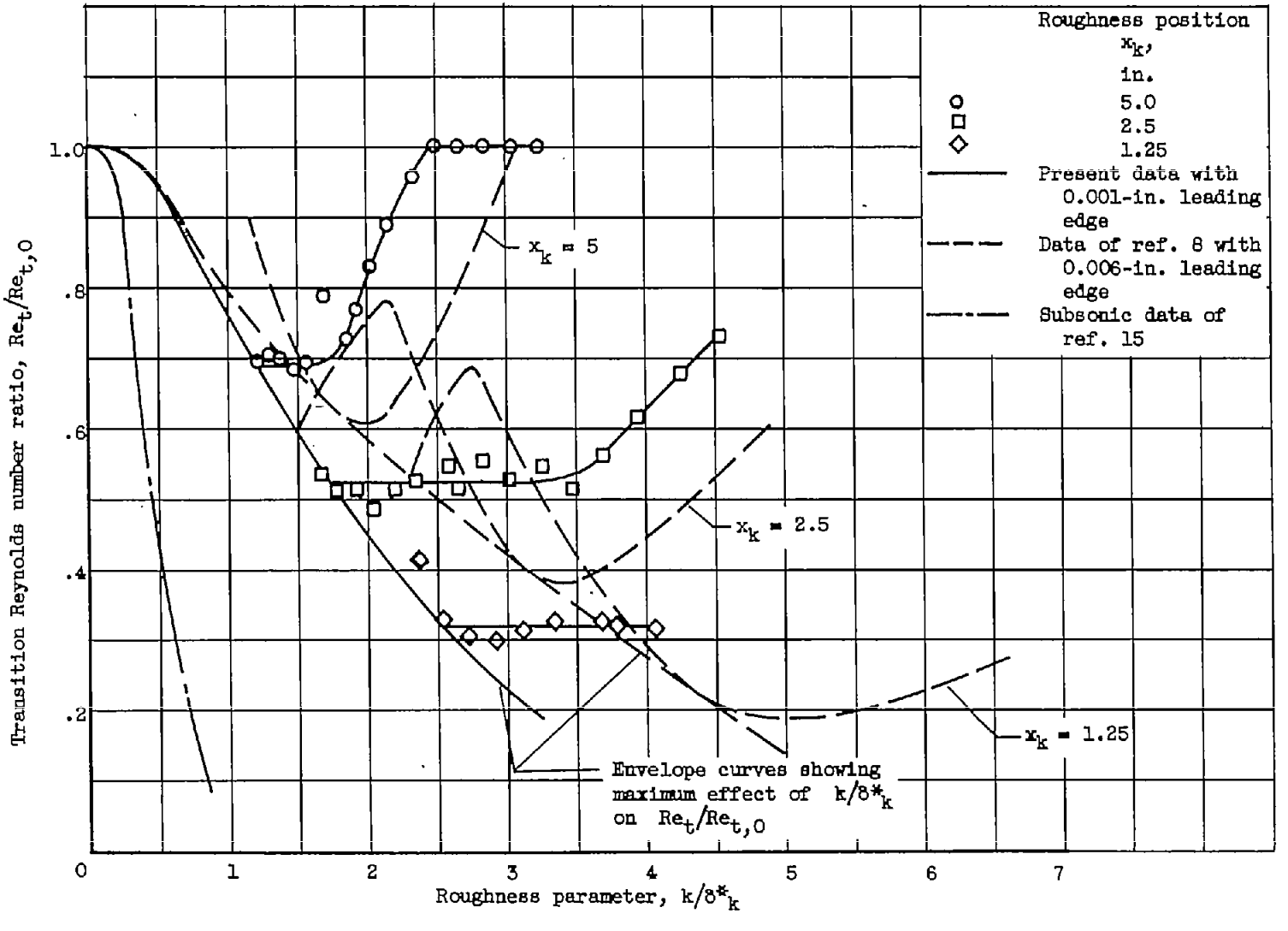

Figure 9. - Effect of roughness parameter on transition Reynolds number ratio.

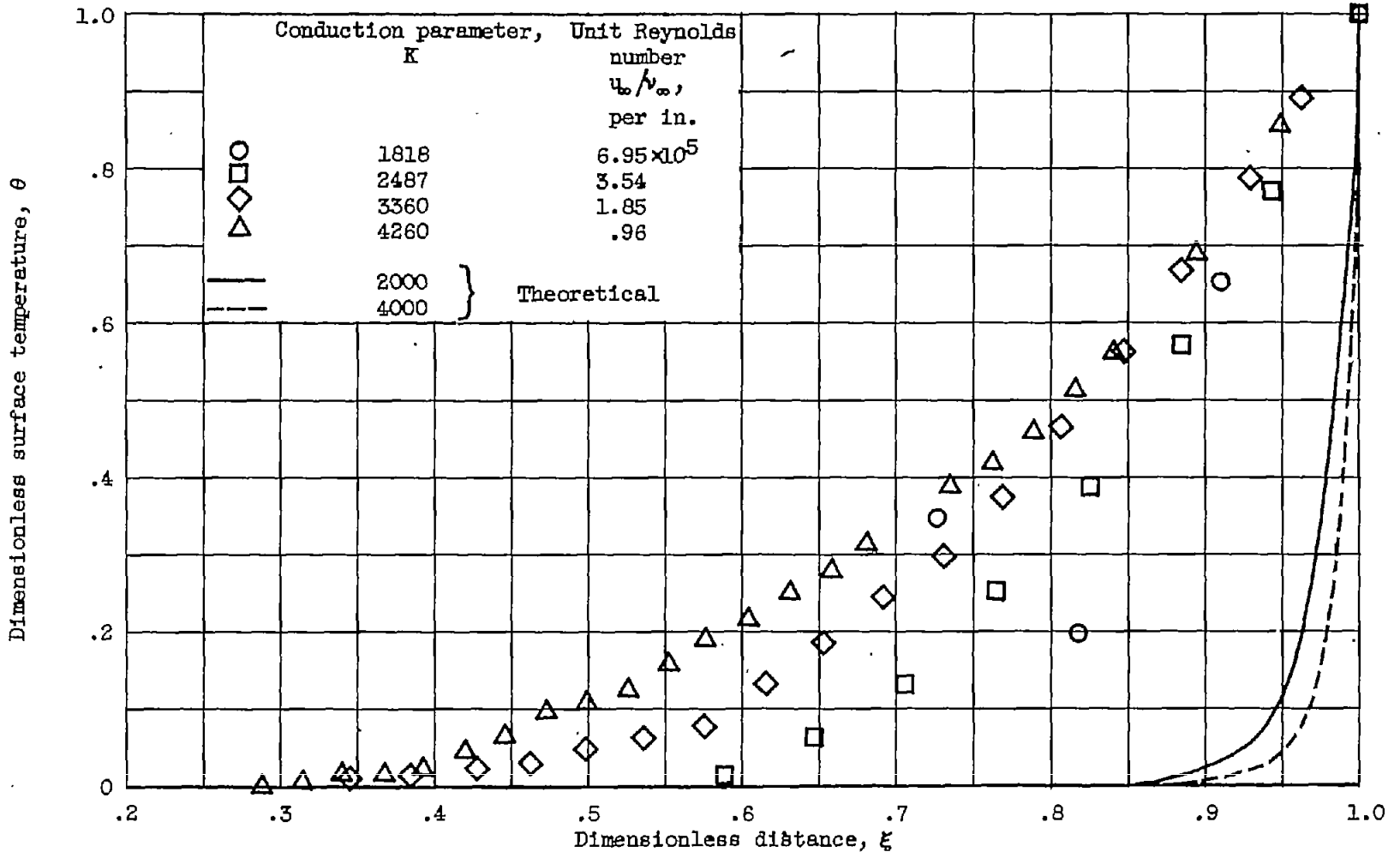

(a) Fiberglas-plastic sleeve.

Figure 11. - Effect of surface conduction on temperature distribution.

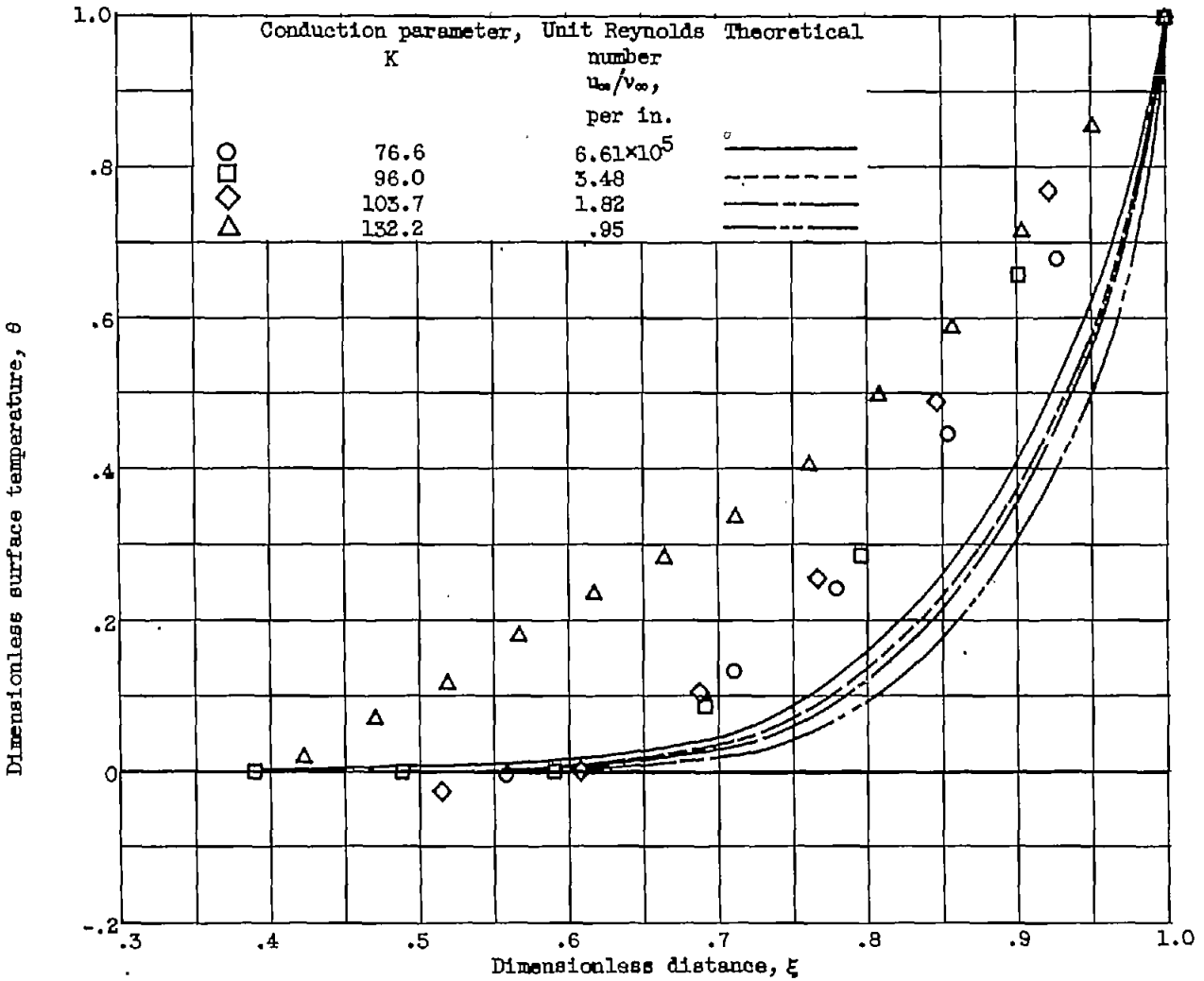

(b) Stainless-steel sleeve.

Figure 11. - Continued. Effect of surface conduction on temperature distribution.

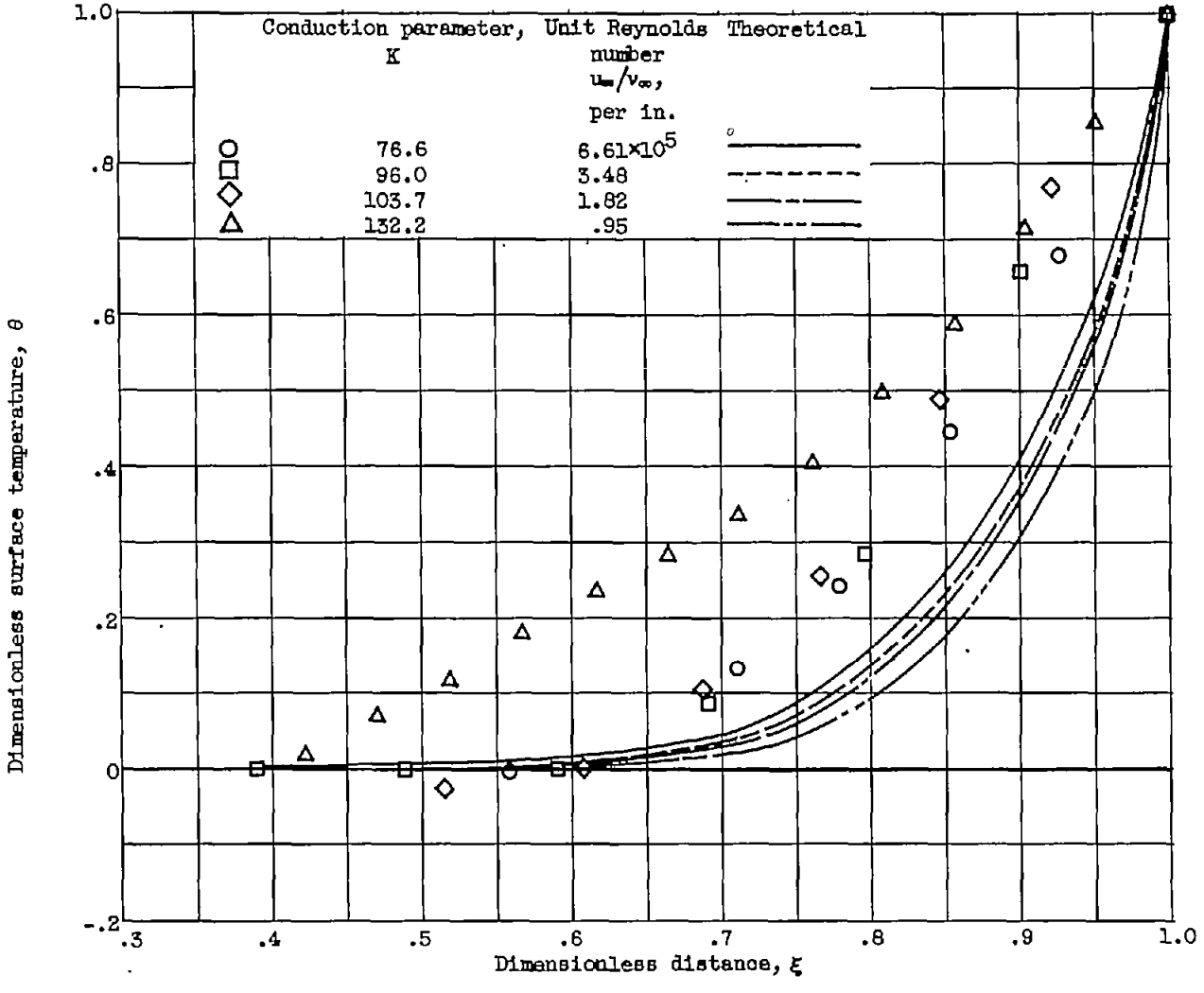

(b) Stainless-steel sleeve.

Figure 11. - Continued. Effect of surface conduction on temperature distribution.

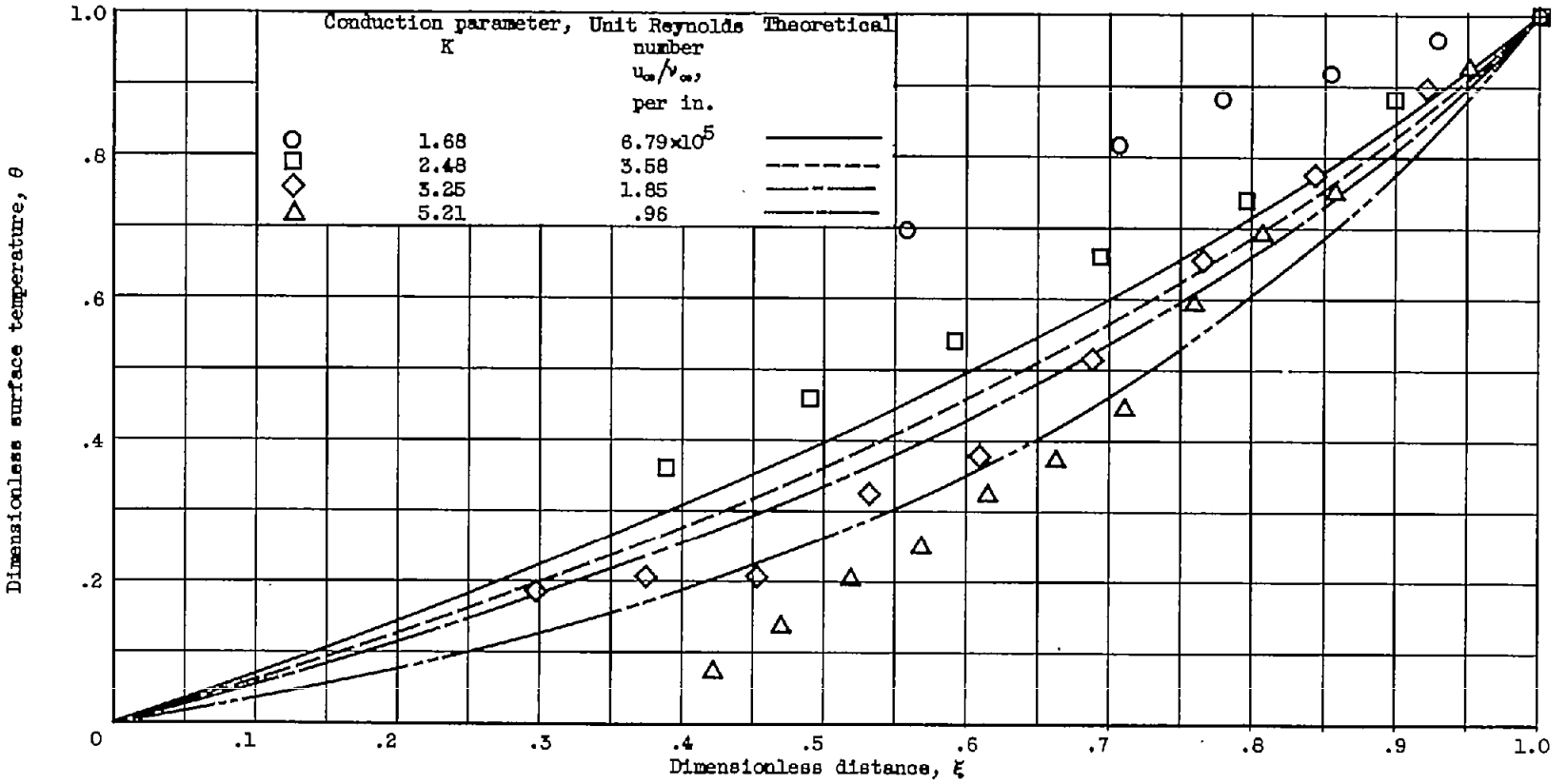

(c) Copper sleeve.

Figure 11. - Concluded. Effect of surface conduction on temperature distribution.

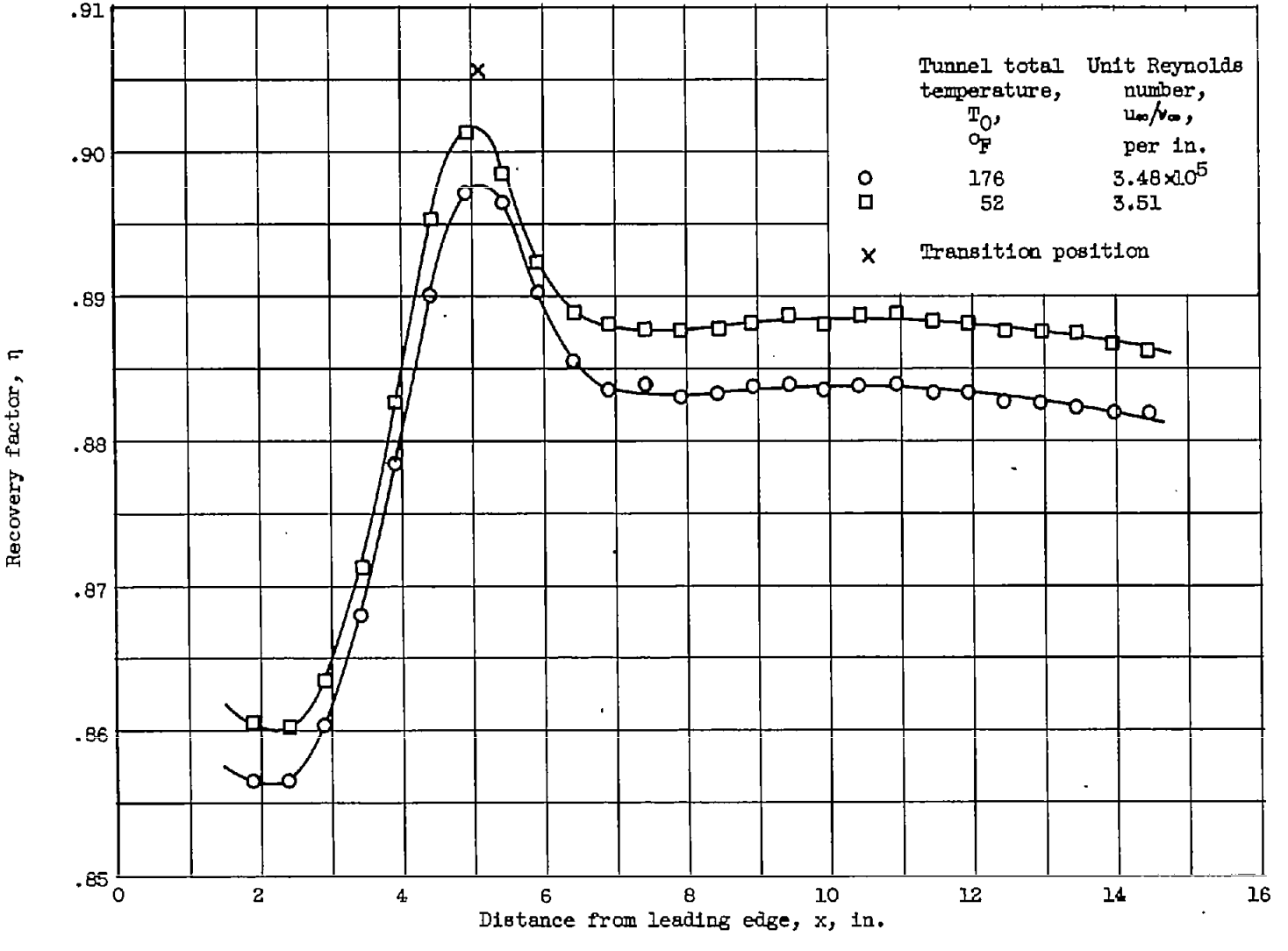

Figure 12. - Effect of stagnation temperature on recovery-factor distributions.

NACA - Langley Field, Va.